Quantum Synchronization in Interacting Non-linear Oscillators

by

Vinayak Narendra Pendse
(Roll No. 20191144)

Project advisor: Prof. Shamik Gupta, TIFR, Mumbai
Expert: Prof. Bijay Aggarwalla, IISER, Pune

March 2024

CERTIFICATE

This is to certify that this dissertation entitled **"Quantum Synchronization in interacting non-linear oscillators"** towards the partial fulfilment of the BS-MS dual degree programme at the Indian Institute of Science Education and Research, Pune represents study/work carried out by **Vinayak Narendra Pendse, IISER, Pune** under the supervision of **Prof. Dr Shamik Gupta, Department of Theoretical Physics, TIFR,** during the academic year **2023-2024**.

Expert: Bijay Agarwalla

Project Supervisor: Shamik Gupta

DECLARATION

I hereby declare that the matter embodied in the report entitled "Quantum Synchronization in Interacting Non-linear Oscillators" are the results of the work carried out by me at the Department of Physics, Indian Institute of Science Education and Research (IISER) Pune, under the supervision of Prof. Shamik Gupta, and the same has not been submitted elsewhere for any other degree. Wherever others contribute, every effort is made to indicate this clearly, with due reference to the literature and acknowledgement of collaborative research and discussions.

Name of Student: Vinayak Narendra Pendse

Roll No: 20191144

ACKNOWLEDGEMENT

I thank everyone who helped me see this project through to completion. I want to express my profound gratitude and deep regard to Prof. Shamik Gupta, Tifr Mumbai, and I sincerely wish to acknowledge his vision, guidance, valuable feedback, and constant support throughout the duration of this project. I would also like to thank all my group members especially Rohitashwa at TIFR for thoughtful discussions and encouragement.

I am indebted to my parents for their steadfast encouragement and time. I am lastly grateful to the Indian Institute of Science Education and Research Pune for providing the necessary resources and facilities to complete this project to the best of my ability.

[Vinayak Narendra Pendse]

March 2024

ABSTRACT

Synchronisation is well studied in Classical limit cycle systems, but synchronisation in the quantum limit cycle systems remains less explored. One such quantum limit cycle oscillator VanderPol oscillator has received much attention in recent years, and a modified version of this oscillator is proposed. We study Synchronisation in two such modified coupled oscillators.

There is much literature on the study of the Open quantum systems, the systems that interact with reservoir. However, the study of such systems in non-markovian conditions remains relatively unexplored. We describe a new way to solve an open quantum system in non-markovian conditions.

Contents

List of Figures

List of Tables

Notations and Abbreviations

No notation is used in this document. No abbreviations have been used either.

1 Introduction

The phenomenon of synchronisation has been a subject of great research in classical systems for decades. The subject lies at the intersection of Statistical Physics and non-linear dynamics. The phenomenon can even be seen in biological systems, such as flocks of birds flying together or fireflies blinking together. It is the interaction between individuals that gives rise to collective phenomenon. A classic example is a bunch of metronomes tuned to different frequencies placed on a single movable platform; after some time, all these metronomes start oscillating in tune. For synchronisation, the individual oscillators must have the property of self-oscillation or, in more technical terms, must have a stable limit cycle. For the existence of a stable limit cycle, both positive and negative damping must be present. The frequency with which it will oscillate around the limit cycle is called its intrinsic frequency. Synchronisation can be studied when a bunch of these oscillators with different frequencies are connected, or we can drive a single oscillator with an external frequency different from that of the oscillator's intrinsic frequency.

The study of synchronisation in quantum systems is relatively new. Quantum systems must have stable limit cycles, too. In quantum systems, positive and negative damping is achieved through interaction with the bath, which is composed of infinite oscillators of all frequencies. Again, synchronisation can be studied in two ways: between oscillators of different frequencies or oscillators connected to an external drive.

What constitutes a valid quantum limit cycle is currently a matter of debate in literature. For example, Spin-half systems are considered non-synchronizable because they do not have a valid limit cycle. On the other hand, they can be shown to have limit cycles if we study the system on a spin-coherent basis. I have explained what spin coherent basis is in the thesis.

Although spin systems aren't the main subjects of our research, the debate is worth noting. The system we will study is a quantum version of the classical VanderPol oscillator. It is, of course, a limit cycle oscillator made possible by positive and negative damping. Because the quantum version needs to be coupled with a bath for damping, the equation of motion we end up solving will be the Lindblad master equation. LME is a general equation for analysing quantum systems by coupling them to the environment(called open quantum systems). While deriving LME, we take several assumptions(details are provided later in the thesis). One such assumption is assuming

Markovian dynamics. Since the system of our interest is an open quantum system, we also explore dynamics with modified LME(with first-order corrections).

The above-asked questions are important in a lot of areas of quantum optics. Like lasers, trapped ion systems. I hope this dissertation sheds some light on some unexplored parts of the subject.

2 Theory

In this section, I will lay down the relevant theory, tools and techniques required in the thesis. We will start with a brief description of a Quantum simple harmonic oscillator, and then I will introduce the relevant theory of open quantum systems and the Wigner distribution function.

2.1 Quantum Simple Harmonic Oscillator

Most readers will be familiar with the quantum SHO, but I will briefly introduce it here because the main system studied in the thesis is built on the SHO. I will also use SHO as an example to describe the tools used for further analysis in the thesis. Consider the following Hamiltonian for SHO written in the form of ladder operators. It is assumed that the reader is familiar with SHO.

$$H = \hbar\omega\left(a^\dagger a + \frac{1}{2}\right)$$
$$a^\dagger = \sqrt{\frac{m\omega}{2\hbar}}\left(x - \frac{ip}{m\omega}\right) \quad a = \sqrt{\frac{m\omega}{2\hbar}}\left(x + \frac{ip}{m\omega}\right) \tag{1}$$

I will use $|\alpha\rangle$ to denote the coherent state, which is an eigenstate of annihilation operator a. The following properties hold for coherent states. For a more detailed analysis of coherent states, please refer to the book[4].

1. $a|\alpha\rangle = \alpha|\alpha\rangle$
2. $|\alpha\rangle = e^{\frac{-|\alpha|^2}{2}} D(\alpha)|0\rangle \qquad D(\alpha) = e^{\alpha a^\dagger - \alpha^* a}$
3. $|\alpha(t)\rangle > = e^{\frac{-i\omega t}{2}} |\alpha e^{-i\omega t}\rangle$

Because of the 3rd property, a coherent state looks like a wave packet oscillating back and forth. To see this, let's consider the expectation values of x and p using $x = \sqrt{\frac{\hbar}{2m\omega}}(a^\dagger + a)$ and $x = i\sqrt{\frac{\hbar m\omega}{2}}(a^\dagger - a)$, we get,

$$\langle x \rangle_{\alpha(t)} = \sqrt{\frac{2\hbar}{m\omega}}|\alpha_0| cos(\omega t - \phi) \tag{2}$$

$$\langle p \rangle_{\alpha(t)} = \sqrt{2m\hbar\omega}|\alpha_0| Sin(\omega t - \phi) \tag{3}$$

In terms of energy eigenstates coherent state can be written as:

$$|\alpha\rangle = e^{\frac{-|\alpha|^2}{2}} \sum_{n=0}^{\infty} \frac{\alpha^n}{\sqrt{n!}}|n\rangle \tag{4}$$

The inner product between two coherent states is:

$$\langle \alpha|\beta\rangle = e^{\frac{-|\alpha|^2}{2} + \frac{-|\beta|^2}{2} + \alpha^*\beta} \tag{5}$$

$$|\langle \alpha|\beta\rangle|^2 = e^{-|\alpha-\beta|^2} \tag{6}$$

2.2 Spin-Coherent states

Now, knowing about SHO coherent states, there is an analogous way to define coherent states for spin systems called Spin-coherent state[11]. Consider Spin-S particle and S_z be the z component of spin. Let $S_- = s_x - iS_y$ using x and y spin components. We define $|0\rangle$ as ground state as follows: $S_Z|0\rangle = S|0\rangle$. it is easy to see:

$$(S_-)^p|0\rangle = \left(\frac{p!2S!}{(2S-p)!}\right)^{\frac{1}{2}}|p\rangle \qquad\qquad 0 <= p <= 2S \tag{7}$$

Where $|p\rangle$ is such that:

$$S_z = (S-p)|p\rangle \tag{8}$$

Consider a state $|\mu\rangle$ which is called spin-coherent states such that:

$$|\mu\rangle = (1+|\mu|^2)^{-S} exp(\mu S_-)|0\rangle \tag{9}$$

You can check by taking the inner product that the state is normalised. and also

$$\langle\lambda|\mu\rangle^2 = \left(1 - \frac{|\lambda-\mu|^2}{(1+|\lambda|^2)(1+|\mu|^2)}\right)^{2S} \tag{10}$$

An alternate way to parameterise, which we will use, is given below: Let $\mu = tan(\frac{1}{2}\theta)e^{i\theta}$, such that $0 <= \theta < \pi$ and $0 <= \phi < 2\pi$.

$$|\theta,\phi\rangle = (cos\frac{\theta}{2})exp\{tan(\frac{\theta}{2}e^{i\phi}S_-)\}|0\rangle \tag{11}$$

For the spin half system, you can think of these states on the bloch sphere, but for higher spins, we have this generalised formalism.

2.3 Quasi-probability distribution

In this section, I will explain the idea behind the Wigner function(also called quasi-probability distribution), and this construction becomes useful later [14]. The idea behind the Wigner function is to define a probability distribution function over phase space. $|\alpha>$ represents the coherent states. We will see later that for quantum harmonic oscillators, using these states as a basis makes sense. For a more detailed explanation, please refer to the book[3].

$$\langle\hat{O}\rangle = \int\int d\alpha d\alpha^* O(\alpha,\alpha^*)W(\alpha,\alpha^*) \tag{12}$$

The way is first to find the characteristic function(the Fourier transform of the Wigner function) and then take the inverse Fourier transform. You can see by the Eq.(12) that characteristic function χ is just the expectation value of $e^{iza+iz^*a^\dagger}$.

$$\langle e^{iza+iz^*a^\dagger}\rangle = \int\int d\alpha d\alpha^* e^{iz\alpha} e^{iz^*\alpha^*} W(\alpha,\alpha^*)$$
$$\langle e^{iza+iz^*a^\dagger}\rangle = \chi = Tr(\rho e^{iza+iz^*a^\dagger}) \tag{13}$$

So, from the density matrix of the state, we can first find the characteristic function and then get the Wigner function by taking the inverse Fourier transform as follows.

$$W(\alpha,\alpha^*) = \int\int dz dz^* e^{-iz^*\alpha^*} e^{-iz\alpha} \chi \tag{14}$$

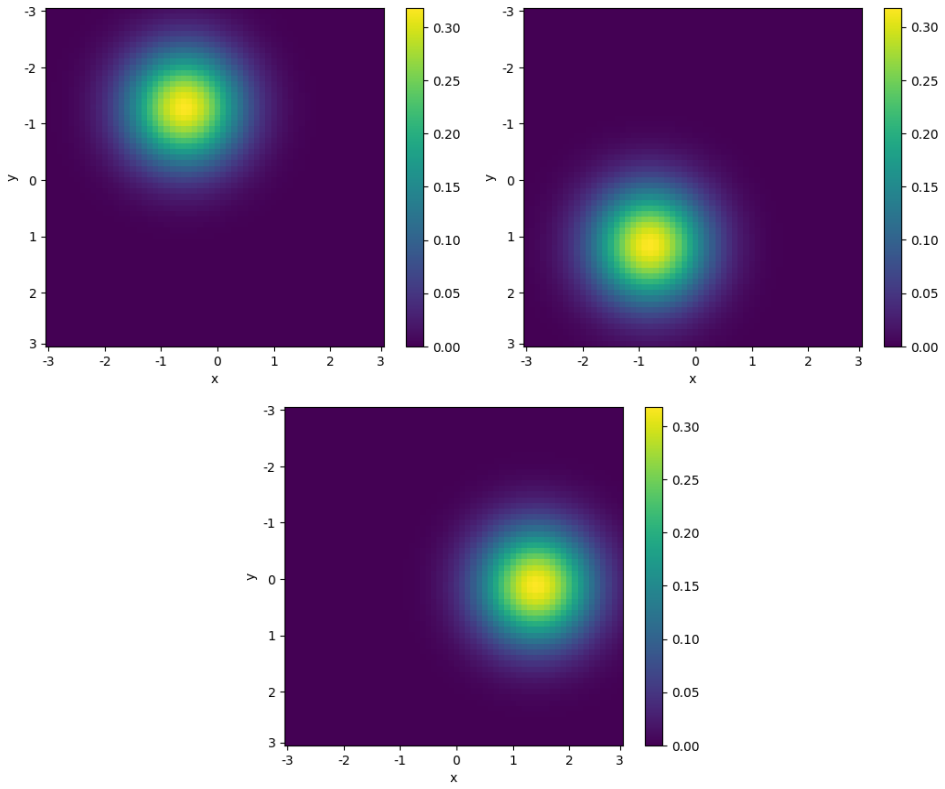

Figure 1: Figure shows Wigner Function Eq. (15) for coherent state of simple Harmonic Oscillator at $T/3, 2T/3$ and T in left, right and bottom respectively. $T = 2\pi\omega_0$ is time period of the oscillation.

The Wigner function is just one of the quasi-probability distribution functions. In Eq.(13) if we change characteristic function to $\chi = Tr(\rho e^{iza} e^{iz^*a^\dagger})$ or $\chi = Tr(\rho e^{iz^*a^\dagger} e^{iza})$ we get different different but equally valid quasi-probability distributions, which are called Husimi-Q and Glauber-P

functions respectively. Wigner function is the most famous, but we can use any of them depending on which is easier to compute.

Corresponding to a density operator ρ characterizing the state of a single degree of freedom in one dimension, the Wigner function in the position-momentum (x, p)-space is defined as

$$W(x,p) = \frac{1}{\pi\hbar}\int_{-\infty}^{\infty} \langle x+y|\rho|x-y\rangle \exp(-2ipy/\hbar)\, dy. \tag{15}$$

Fig. 1 shows the Wigner function of a coherent state at different times. Note that the Wigner function of the coherent state is a Gaussian (given by $W(\alpha,\alpha^\star) = (2/\pi)\exp(-|\alpha-\alpha_0 e^{-i\omega t}|^2)$), whose centre revolves around the origin with a time period equal to $2\pi/\omega_0$, where ω_0 is the frequency of SHO.

2.4 Open Quantum Systems

The system we are studying in the thesis comes under a class systems called the open quantum system. These are systems that are not isolated and interact with the environment. There is a well-established way to analyse such systems. Below, I have laid down a brief derivation to get the equation for the time derivative of the density operator. The derivation is a bit involved. Complete derivation can be found in this book [3]. We start by writing down the complete Schrodinger equation for the system and bath and then trace out the bath degrees of freedom to end up with the equation only for the system Density operator. To make calculations easier, we go into the 'interaction picture'. Let the complete Hamiltonian be,

$$H_{Total} = H_S + H_B + H_I$$

$$H_S = \omega_0 a^\dagger a, \qquad H_B = \Sigma_k \omega_k b_k^\dagger b_k, \qquad H_I = a\Gamma^\dagger + a^\dagger\Gamma \qquad \Gamma = \Sigma_j \omega_j k_j b_j$$

Here, $a, a^\dagger$ are ladder operators of the system and $b_k, b_k^\dagger$ are ladder operators of the bath. The interaction Hamiltonian represents a one-photon gain or loss, i.e. the photon goes from system to bath or bath to system. Let χ be the density operator of the system and bath, and ρ and R be system and bath density operators resp. Below are the assumptions made to derive the final equation

1. System and environment interaction is only turned on at t = 0, i.e. $\chi(0) = \rho(0)\otimes R(0)$

2. $tr_E[\tilde{H}_I(t), \rho(0)] = 0$ .This can always be achieved.

3. Born approximation. This is only possible when the environment is large, and interaction Hamiltonian is weak.

4. Markov approximation. This is only possible when the environment's evolution time is much smaller than the system's evolution time scale.

Assuming you are already familiar with the Heisenberg picture(HP), the Interaction Picture(IP) is a combination of the Schrodinger picture(SP) and the Heisenberg picture. That is, we let H_s and H_B evolve the operators(HP) and let H_I evolve the state of the system(SP). Let, for any operator O,

$$\tilde{O} = e^{i(H_s+H_B)t} O e^{-i(H_s+H_B)t}$$

Now, the evolution of the density operator in the interaction picture is given as follows.

$$\dot{\tilde{\chi}} = -i\left[\tilde{H}_I(t), \tilde{\chi}\right] \tag{16}$$

Now, integrate Eq.(16) we get,

$$\tilde{\chi}(t) = \chi(0) - i\int_0^t dt' \left[\tilde{H}_I(t'), \tilde{\chi}(t')\right] \tag{17}$$

Substituting back, we get,

$$\dot{\tilde{\chi}} = -i\left[\tilde{H}_I(t), \tilde{\chi}(0)\right] - \frac{1}{\hbar^2}\int_0^t dt' \left[\tilde{H}_I(t), \left[\tilde{H}_I(t'), \tilde{\chi}(t')\right]\right] \tag{18}$$

In the above equation, we take partial trace over bath and using assumption '2', we get,

$$\dot{\tilde{\rho}} = -\frac{1}{\hbar^2}\int_0^t dt' Tr_{bath}\{\left[\tilde{H}_I(t), \left[\tilde{H}_I(t'), \tilde{\rho}(t')R_0\right]\right]\} \tag{19}$$

Put in the interaction Hamiltonian and expand the commutator, we get the following. (H.C. means hermitian conjugate)

$$\dot{\tilde{\rho}} = -\int_0^t dt' \{ \left[\tilde{a}(t)\tilde{a}^\dagger(t')\tilde{\rho}(t') - \tilde{a}^\dagger(t')\tilde{\rho}(t')\tilde{a}(t) \right] \langle \tilde{\Gamma}^\dagger(t)\tilde{\Gamma}(t') \rangle_{bath} + H.C. \\ + \left[\tilde{a}^\dagger(t)\tilde{a}(t')\tilde{\rho}(t') - \tilde{a}(t')\tilde{\rho}(t')\tilde{a}^\dagger(t) \right] \langle \tilde{\Gamma}(t)\tilde{\Gamma}^\dagger(t') \rangle_{bath} + H.C. \} \tag{20}$$

To get this, we have used the following, where $n(\omega, T) = \dfrac{e^{-\hbar\omega/T}}{1 - e^{-\hbar\omega/T}}$

$$\langle \tilde{\Gamma}(t)\tilde{\Gamma}^\dagger(t') \rangle_{bath} = \sum_j |k_j|^2 e^{-i\omega_j(t-t')} \left(n\left(\omega_j, T\right) + 1 \right) \\ \langle \tilde{\Gamma}(t)\tilde{\Gamma}^\dagger(t') \rangle_{bath} = \sum_j |k_j|^2 e^{-i\omega_j(t-t')} n\left(\omega_j, T\right) \\ \langle \tilde{\Gamma}(t)\tilde{\Gamma}(t') \rangle_{bath} = \langle \tilde{\Gamma}^\dagger(t)\tilde{\Gamma}^\dagger(t') \rangle_{bath} = 0 \tag{21}$$

Now, this is where we apply Markovian approximation as follows,

$$\langle \tilde{\Gamma}(t)\tilde{\Gamma}^\dagger(t') \rangle_{bath} = (R_1 + iI_1)\delta(t - t') \tag{22}$$

$$\langle \tilde{\Gamma}^\dagger(t)\tilde{\Gamma}(t') \rangle_{bath} = (R_2 + iI_2)\delta(t - t') \tag{23}$$

Therefore, we no longer have the integral, and if you simplify the equation and then go back to the Shrodienger Picture, we get the following equation, which is called the Lindblad Master equation, where $w' = w_0 + I_1 - I_2$ and $D[O]\rho = 2O\rho O^\dagger - \{O^\dagger O, \rho\}$

$$\dot{\rho} = -iw'[a^\dagger a, \rho] + R_1 D[a^\dagger]\rho + R_2 D[a]\rho \tag{24}$$

The interaction of the harmonic oscillator with the reservoir occurs via the exchange of photons. The terms $D[a^\dagger]\rho$ and $D[\hat{a}]\hat{\rho}$ denote one-photon gain and one-photon loss, respectively. More generally, a term $D[O]\rho$ appearing in the Lindblad equation of an open quantum system interacting with a reservoir physically represents processes resulting in the system jumping from $|I\rangle$ to $|F\rangle$ given by $|F\rangle = O|I\rangle$, justifying the operator O being referred to as a jump operator [2].

Quantum Monte Carlo Wave Function

This is a stochastic process that simulates any general Open Quantum system. Lindblad equation is an ODE, so you might think simple Euler or RK-4 would suffice, but this becomes computationally very expensive. QMCWF is much faster.

Let a general Lindbladian be as follows,

$$\dot{\rho} = -\frac{i}{\hbar}[H_0, \rho] + \sum_{i=1}^{N} \gamma_i \left(L_i \rho L_i^\dagger - \frac{1}{2} \left\{ L_i^\dagger L_i, \rho \right\} \right) \tag{25}$$

Below is the general procedure for simulating. Let the Hamiltonian for the system be H_0, and L_k be the jump operators. We can think of the evolution of the state as a stochastic process, where if currently, the system is in state $|\psi>$, it will jump to $L_k|\psi>$ with probability dp_k/dp (as defined below in step 1) and the system shows simple Liouville evolution with probability $1-dp$(as defined in step 1).

$$H = H_0 - \frac{i}{2}\Sigma_k {L_k}^\dagger L_k$$

. But this Liouville evolution will be with modified Hamiltonian given by:

Algorithm:

1. $dp = \Sigma_k dp_k$, where $dp_k = dt < \psi|{L_k}^\dagger L_k|\psi >$
2. $0 <= \varepsilon <= 1$, generate uniform random number.
3. if $\varepsilon < dp$ then $|\psi > \rightarrow \frac{L_k|\psi>}{\sqrt{\frac{dp_k}{dt}}}$, where k is randomly chosen with probability $\frac{dp_k}{dp}$.
4. else $|\psi > \rightarrow \frac{e^{-iHdt}}{\sqrt{1-dp}}|\psi >$
5. Goto 1

For simplicity, let's simulate a system with just two levels connected to a bath using this algorithm. A two-level system could be anything, but for the sake of illustration, we will take a spin-half system in an external magnetic field with the following Hamiltonian.

$$H_{Total} = H_S + H_B + H_I$$

$$H_S = \omega_0 \sigma_z, \qquad H_B = \Sigma_k \omega_k b_k^\dagger b_k, \qquad H_I = \sigma_- \Gamma^\dagger + \sigma_+ \Gamma \qquad \Gamma = \Sigma_j \omega_j k_j b_j$$

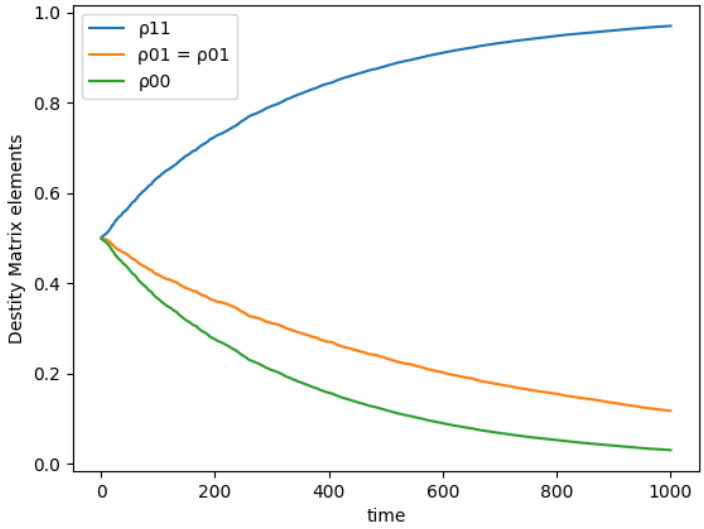

Figure 2: Figure shows results of simulating Eq. (25) using QMCWF. We have used a single jump operator with $\gamma_1 = 0.3$, and we start the system with equal superposition of ground and excited state.

We start with the initial state, which is an equal combination of ground and excited state, $|\psi\rangle = \frac{1}{\sqrt{2}}(|g\rangle + |e\rangle)$. Fig. 2 shows the results.

2.5 Classical Rayleigh-VanderPol oscillator

Rayleigh-VanderPol is a class of classical oscillators which are SHO with non-linear damping. Consider the following equation [1],

$$\ddot{x} + x - \varepsilon\dot{x} + \gamma_3(\eta x^2 + \zeta\dot{x}^2)\dot{x} = 0 \tag{26}$$

The above equation represents (a): Rayleigh oscillator for $\eta = 0, \zeta = 1$, (b): VanderPol oscillator for $\eta = 1, \zeta = 0$, (c): Rayleigh-VanderPol oscillator for $\eta = 1, \zeta = 1$. In the limit of weak ε, there is an approximate way to solve the equation called Secular Perturbation Theory. Consider the following ansatz.

$$x(t) = \frac{1}{2}(A(T)e^{-it} + c.c.) + \varepsilon x_1(t) + o(\varepsilon^2), T = \varepsilon t \tag{27}$$

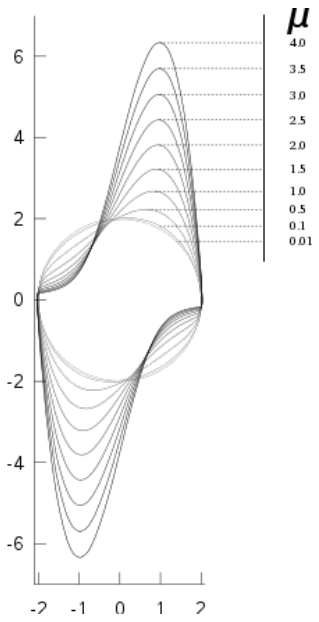

Figure 3: Steady state limit cycle for vdPo at different non-linearity parameters μ.

Here, T is the slow time scale, and t is the fast time scale. This type of solution is only valid when non-linearity is small, and we can think of time scale separation. So, on a small time scale, motion is basically simple Harmonic, and on a large time scale, we simply modulate the amplitude of this simple Harmonic motion. Now, putting back the Ansatz in the original equation, we get the following solution for $A(T)$, and it can be seen that the correction term proportional to ε is small.

$$\frac{dA}{dT} = \frac{1}{2}\left(1 - \frac{\eta + 3\zeta}{4A_c^2}|A|^2\right)A, \qquad A_c = \sqrt{\frac{\varepsilon}{\gamma_3}} \tag{28}$$

From Eq.(28), it is clear that there will be a limit cycle. Having a limit cycle becomes very important as it is a necessary condition for Synchronisation. Below are radii of oscillation in a steady state that we get by putting LHS of Eq.(28) equal to zero.

$$|A| = \frac{2A_c}{\sqrt{\eta + 3\zeta}} \tag{29}$$

Fig.3 shows the limit cycles in the steady state for the different values of $\varepsilon(\mu$ in the diagram). Note that the limit cycle becomes more and more non-circular as we increase non-linearity. Quantum model vdPo should be able to capture this effect.

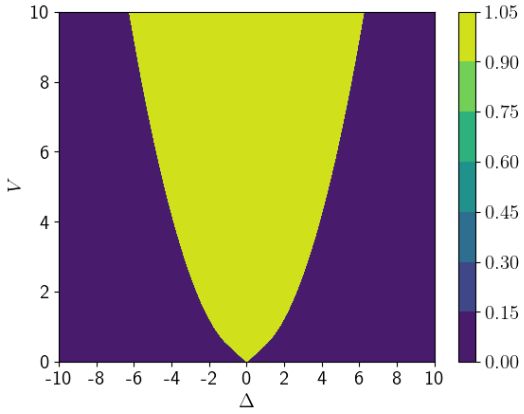

Figure 4: Figure shows the region where the coupled oscillators are synchronised. The yellow region is synchronised. On the x-axis, there is the detuning parameter, and on the y-axis, there is coupling strength.

2.5.1 Synchronisation in coupled classical VanderPol oscillators

Let us now couple two oscillators of the form Eq.(28) with dissipative coupling. Please refer to the Appendix [A]. For easier analysis, we will go in the polar frame of reference and redefine variables as follows[8].

$A_i = r_i e^{i\theta_i},\ \Delta = \omega_1 - \omega_2,\ \theta = \theta_1 - \theta_2$

$$\begin{aligned} \dot{r}_1 &= r_1(k_1 - 2k_2 r_1^2) - V(r_1 - r_2 cos\theta) \\ \dot{r}_1 &= r_2(k_1 - 2k_2 r_2^2) - V(r_2 - r_1 cos\theta) \\ \dot{\theta} &= -\Delta - V\left(\frac{r_1}{r_2} + \frac{r_2}{r_1}\right) sin\theta \end{aligned} \tag{30}$$

From the equation in polar form, you can see in the steady that state because the value of sine has to be between (-1,1); for a given , there is a critical V_c beyond which $\dot{\theta} = 0$, this is called **Synchronisation.** Keep in mind this equation; in the following chapters, we build a quantum version of the oscillator. Fig.4 called Arnold tongue shows the region in which the oscillators are synchronised. Higher coupling strength is required to synchronise oscillators with higher detuning (Δ).

2.6 Quantum VanderPol oscillator

Quantum VanderPol is a quantum version of classical vanderPol. Such a model was originally proposed by Lee-Sadeghpour Ref. [9]. Below is the Lindblad master equation representing the quantum VanderPol [1].

$$\dot{\rho} = -i[H_0, \rho] + \gamma_1 D[a^\dagger]\rho + \gamma_2 D[a]\rho + \gamma_3 D[a^2]\rho \qquad H_0 = \omega_0 a^\dagger a \tag{31}$$

$$D[O]\rho = 2O\rho O^\dagger - \{O^\dagger O, \rho\} \tag{32}$$

This is a simple harmonic oscillator connected to a bath. Interaction with bath is given by $D[a^\dagger]\rho$,$D[a]\rho$ and $D[a^2]\rho$, which are one-photon gain, one-photon loss and two-photon loss terms respectively. And $H_0 = \omega_0 A^\dagger a$ is Hamiltonian for SHO.

To see that this becomes the classical equation in high energy limit, calculate $\frac{d}{dt}\langle a\rangle = Tr[\dot{\rho}a]$. The expectation value of the annihilation operator becomes α in the semi-classical limit. Below is proof that it returns Eq.(28). In the above expectation value equation, put in $\dot{\rho}$ from Eq.(31) we get,

$$\langle \dot{a}\rangle = -i\langle a\rangle + \frac{\gamma_1 - \gamma_2}{2}\langle a\rangle - \gamma_3\langle (a^\dagger a)a\rangle \tag{33}$$

In the above equation, in high energy limit $\langle a\rangle \sim \alpha$ and $\langle (a^\dagger aa)\rangle \sim |\alpha|^2\alpha$ and $\varepsilon = \gamma_1 - \gamma_2$ therefore we get,

$$\frac{d\alpha}{dt} = -i\alpha + \frac{\varepsilon}{2}(1 - \frac{2|\alpha|^2}{A_c^2})\alpha \tag{34}$$

Now, go into a slow-moving scale to return to the classical equation.

$$\alpha(t) = \frac{A(T)}{\sqrt{2}}e^{-it}, T = \varepsilon t \tag{35}$$

So, in terms of A we get,

$$\frac{dA}{dt} = \frac{1}{2}\left(1 - \frac{|A|^2}{A_c^2}\right)A \tag{36}$$

As you can see, we almost get back to the form of classical vdPo in Eq. 28 (recall that for VdPo $\eta = 1\zeta = 0$). Because we don't get back exactly the same equation, this model fails to capture that the limit cycle of classical vdPo loses rotational symmetry if we increase the value of ε. In the

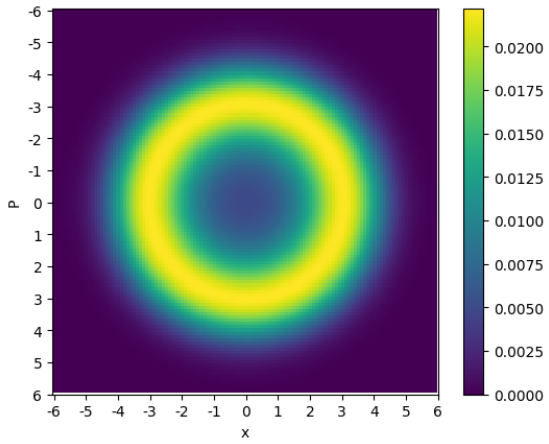

Figure 5: The figure shows the Wigner Function computed for the steady state of the old quantum vdPo due to Lee. Parameters taken for the simulation are $\gamma_1 = 1, \gamma_2 = 0, \gamma_3 = .01$ Note that the peak of the function traces the limit cycle of classical vdPo. The limit cycle remains rotationally symmetric.

coming section, I will describe the new model of quantum vdPo(due to Arosh), and we will study synchronisation in two such coupled oscillators.

2.7 Modified quantum VanderPol oscillator

$$\dot{\rho} = -i[H_0, \rho] + \gamma_1 D[a^\dagger]\rho + \gamma_2 D[a]\rho + \gamma_3 D[xa]\rho, \qquad H_0 = \omega_0 a^\dagger a \tag{37}$$

This is the recent quantum vdPo model due to Arosh[1]. The difference is in the two-photon loss term. In the older model, it was a^2. Here, it is xa, which will give rise to non-diagonal terms in the density matrix, giving rise to coherence. Because of the non-diagonal terms, we will get the Wigner function that isn't rotationally symmetric. We can do a similar analysis as in Eq.33 to get the corresponding classical equation similar to Eq.36. Please refer to the Appendix [C]

$$\frac{d\alpha}{dt} = -i\alpha + \frac{\varepsilon}{2}\left(1 - \frac{2\langle x\rangle^2}{A_c^2}\right)\alpha \tag{38}$$

Now, go into a slow-moving scale to return to the classical equation.

$$\alpha(t) = \frac{A(T)}{\sqrt{2}} e^{-it}, T = \varepsilon t \tag{39}$$

So, in terms of A we get,

$$\frac{dA}{dt} = \frac{1}{2}\left(1 - \frac{\langle x\rangle^2}{2A_c^2}\right)A \tag{40}$$

We can write $\alpha = \langle \hat{a} \rangle = \langle x \rangle - i\langle p \rangle$ and use Eq. 38 to get the following equations by separating the real and the imaginary parts,

$$\langle \dot{x} \rangle = \frac{\varepsilon}{2}\left(1 - \frac{\langle x\rangle^2}{2A_c^2}\right)\langle x \rangle + \langle p \rangle, \tag{41}$$

$$\langle \dot{p} \rangle = \frac{\varepsilon}{2}\left(1 - \frac{\langle x\rangle^2}{2A_c^2}\right)\langle p \rangle - \langle x \rangle, \tag{42}$$

where, $\varepsilon = \gamma_1 - \gamma_2$. Now taking another time derivative of Eq. 89 and substituting $\langle \dot{p} \rangle$ from Eq. 90 we get the following equation,

$$\langle \ddot{x} \rangle + \langle x \rangle = \varepsilon\left(1 - \frac{\langle x\rangle^2}{2A_c^2}\right)\langle \dot{x} \rangle + \mathscr{O}\left(\varepsilon^2\right). \tag{43}$$

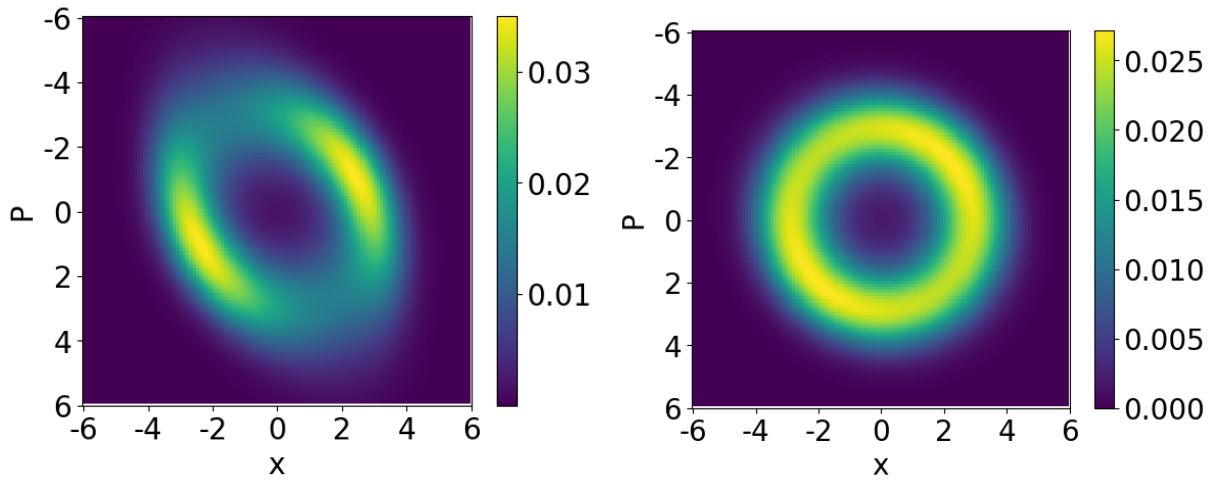

Figure 6: The figure shows the density plot for the Wigner function $W(x,p)$ for the single quantum van der Pol oscillator, Eq. (38), with $\gamma_1 = 0.5, \gamma_3 = 0.125$ (left panel), and $\gamma_1 = 0.05, \gamma_3 = 0.0125$ (right panel), while $\gamma_2 = 0.0$ for both the panels. **Message: one may get either a symmetric or an asymmetric shape depending on the parameter values; compare with Lee-Sadeghpour model that generates only symmetric shapes.**

Eq. 91 is the classical van der Pol oscillator upto $\mathscr{O}\left(\varepsilon^2\right)$, where the non-linearity parameter ε corresponds to $\gamma_1 - \gamma_2$ while $2\frac{\gamma_1-\gamma_2}{\gamma_3}$ is the amplitude of the limit cycle. This model can capture the rotational asymmetry in the limit cycle. Fig. 6 shows the Wigner function of the steady state density matrix, and Fig.7 shows the density matrix elements. As you can see, non-diagonal elements

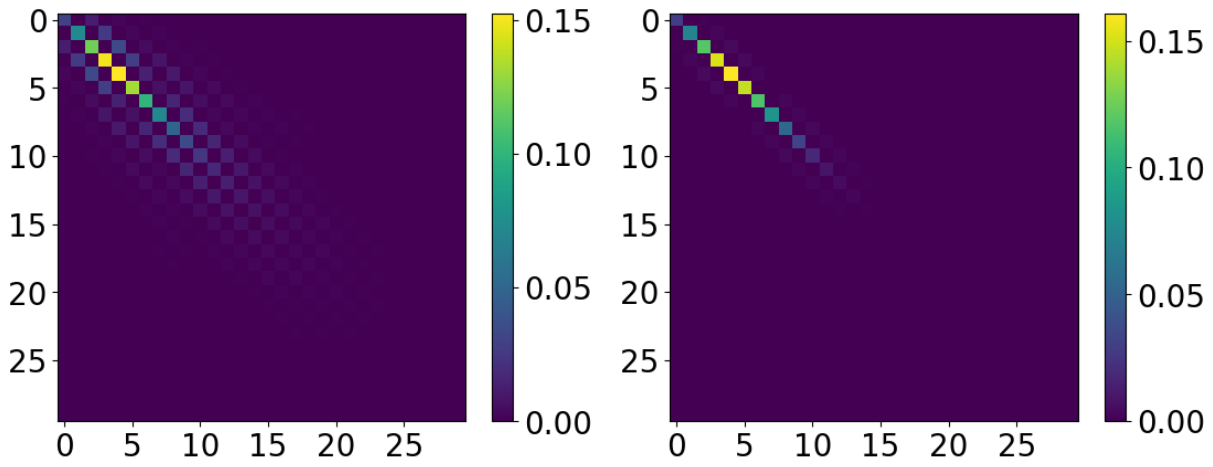

Figure 7: Corresponding to the plots in 6, the figure shows the structure of the density matrix, with the same values of the parameters $\gamma_1, \gamma_2, \gamma_3$. Unlike the right panel, one may observe non-zero off-diagonal elements in the density matrix shown in the left panel. **Message: when seen in conjunction with panel (a), we conclude that the off-diagonal elements are the ones that serve to generate the asymmetric shape.**

in the density matrix make the Wigner function rotationally asymmetric.

Now we are ready to study synchronisation in two improved coupled quantum vdPos. The coupling we will be using is common in the literature, along the lines of [8]. This type is called diffusive coupling. Below is the Lindblad master equation for this system where $H_j = \omega_j a^\dagger a$.

$$\frac{d\rho}{dt} = \sum_{j=1}^{2} \left(-i[H_j, \rho] + \gamma_1 D[a_j^\dagger]\rho + \gamma_2 D[a_j]\rho + \gamma_3 D[x_j a_j]\rho \right) + V D[a_1 - a_2]\rho. \tag{44}$$

We use this because if we do semi-classical analysis similar to Eq.33 and Eq.36, we get coupling term similar to that in Eq.30. Throughout the thesis, we will deal with the case of $\gamma_2 = 0$.

3 Results and discussion

There are two main results in the thesis. First are the results on the synchronisation of quantum vdPo. Second, the results of first-order correction to the Lindblad master equation are used to get the non-markovian evolution in time for the density operator. The former has already been studied in the older model, but because the newer model is better, it is interesting to study synchronisation in the new model. The non-markovian result is completely new, and rather than synchronisation, I have shown results of the time of evolution for spin systems.

3.1 Analysis of Quantum coupled VanderPol

In classical physics, the definition and physical interpretation of synchronisation is very clear. When oscillators are synchronised, they are either phase-locked or the relative phase difference doesn't change with time. Because quantum SHO isn't exactly a phase oscillator, this type of definition can't be used, so it is clear that we have to come up with a way to get phase from a quantum oscillator and come up with a way to measure synchronisation. The former can be solved by using coherent states as your basis as they come closest to making quantum SHO into a phase oscillator. For the latter, there isn't much consensus in the literature. We will use Power Spectrum as described in [12] and Generalised Measure of Synchronisation as described in [5].

The system's quantum limit(i.e., low energy limit) can only be solved numerically. We have used the Python package called Qutip[6] for the simulation and plots. In semi-classical Limit(i.e. high energy limit), we can solve the system to get the time evolution of the Wigner function of the system analytically. This is important to show the crucial property of amplitude death observed in classical vdPo is also observed in quantum vdPo. In the next section, I have laid down the procedure to evolve the Wigner distribution in time, and I have shown plots showing the death amplitude.

3.1.1 Semiclassical Description using a Fokker-plank equation

From the previous section, recall the discussion on the quasi-probability distributions. There are three different quasi-probability distributions possible. The characteristic function associated with the Wigner distribution is called χ_s, the one for Glauber-P is called χ_N, and the one for Husimi-q is

called χ_A. We will calculate χ_N first and then convert it χ_s using relation $\chi_s = e^{\frac{-|z|^2}{2}}\chi_N$(Not getting into the derivation of the relation here) and then finally take inverse Fourier transform to get the Wigner function. The derivation is straightforward but long; it is provided in the Appendix B . Here, I will write down the final equation and the simulation results.

$$\begin{aligned}\frac{d\rho}{dt} = &\sum_{j=1}^{2}\left(-i[H_j,\rho] + \gamma_1 D[a_j^\dagger]\rho + \gamma_2 D[a_j]\rho + \gamma_3 D[x_j a_j]\rho\right)\\ &+ VD[a_1 - a_2]\rho. \end{aligned} \tag{45}$$

For the above Lindblad Dynamics with $H_j = \omega_j a^\dagger a$, corresponding Wigner distribution dynamics reduces to the form of the Fokker-Plank equation in semi-classical limit given as,

$$\begin{aligned}\frac{\partial W}{\partial t} = \sum_{j=1}^{2}\Bigg[&-\left(\partial_{\alpha_j}\mu_{\alpha_j} + c.c.\right) + \frac{1}{2}\Bigg(\frac{\partial^2 D_{\alpha_j^2}}{\partial \alpha_j^2}\\ &+ \frac{\partial^2 D_{\alpha *_j^2}}{\partial \alpha *_j^2} + \frac{\partial^2 D_{\alpha_j \alpha *_j}}{\partial \alpha_j \partial \alpha *_j} + \frac{\partial^2 D_{\alpha_j \alpha *'_j}}{\partial \alpha_j \partial \alpha *'_j}\Bigg)\Bigg] W(\alpha, \alpha^*).\end{aligned} \tag{46}$$

Here, $j' = 2$ whenever $j = 1$ and vice versa. The coefficients are given by,

$$\begin{aligned}\mu_{\alpha_j} &= \left(-i\omega_j + \frac{\gamma_1}{2} - \frac{V}{2}\right)\alpha_j + \frac{V}{2}\alpha_{j'},\\ &\quad - \frac{\gamma_3}{2}\left(\alpha^3 + \alpha^*|\alpha|^2 + 2\alpha|\alpha|^2\right),\\ D_{\alpha_j \alpha_j^*} &= \gamma_1 + V + \frac{\gamma_3}{2}\left(\alpha_j^{*2} + \alpha^2 + 3|\alpha|^2\right),\\ D_{\alpha_j \alpha *_{j'}} &= V,\\ D^2_{\alpha_j} &= \frac{-\gamma_3}{2}\left(\alpha^2 + 2|\alpha|^2\right),\\ D_{\alpha_j^{*2}} &= c.c.\text{ of } D_{\alpha_j^2}.\end{aligned} \tag{47}$$

μ_{α_j} gives the elements of the drift vector, while $D_{\alpha_j}, D_{\alpha_j^*}, D_{\alpha_j \alpha *_j}$, and $, D_{\alpha_j \alpha *'_j}$ give the elements of the diffusion matrix.

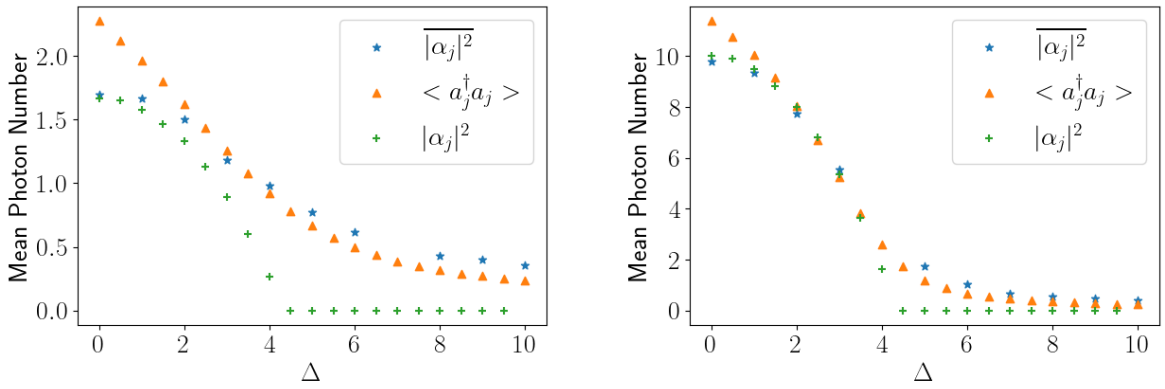

Figure 8: The figure shows the relation between the photon number and detuning parameter given by Δ in the semi-classical limit, with $\gamma_1 = 1.0, \gamma_3 = 0.3$ (left panel) and $\gamma_1 = 1.0, \gamma_3 = 0.05$ (right panel). The three plots in each panel refer to (i) the quantum system, Eq. (44), with the results obtained by using the Fokker-Planck description, (ii) the quantum system, Eq. (44), with the results obtained by employing QuTip, and (iii) the classical system, Eq. (85). **Message: Higher the ratio γ_1 to γ_3, closer to the classical-system results are the results obtained for the quantum system using the Fokker-plank equation. You can clearly see that in the high energy limit (figure on the right) results from Fokker-plank dynamics are better than Qutip.**

Then as outlined in Appendix B we solve the corresponding stochastic differential equation numerically to obtain the average photon number for a given detuning parameter ($\Delta = \omega_2 - \omega_1$). We plot our results in Fig. 8. The figure contains three curves: (i) $\langle a_j^\dagger a_j \rangle$ is obtained by numerically from Eq. (44) in the steady state, (ii) $\overline{|\alpha_j|^2}$ is obtained by numerically integrating Eq. (46) and averaging over 10,000 independent realizations, and (iii) $|\alpha_j|^2$ is obtained by numerically integrating the (noiseless) classical vdPo in Eq (30) till the system reaches a steady state. We have the following observations:

- In the high energy limit, simulating using Qutip becomes computationally expensive. But as you can see, results from Fokker-plank dynamics match well with the classical vdPo, making the Fokker-plank equation and corresponding stochastic dynamics a viable alternative.

- In the low energy limit, however, results from Fokker-plank dynamics are not a good match. But in this limit Qutip is computationally viable.

- Interestingly, the difference between $|\alpha_j|^2$ and the other two curves— representing $\langle a_j^\dagger a_j \rangle$ and $\overline{|\alpha_j|^2}$— increases as the difference between γ_1 and γ_3 decreases. This indicates that

in low energy limit photon number for quantum vdPo is different from the classical vdPo indicating presence of quantum fluctuations.

3.2 Emergence of Synchronisation

We have already shown that quantum vdPo shows the property of amplitude death; we are now ready to study synchronisation. As mentioned earlier, let's start with a description of the first order-parameter Power Spectrum.

3.2.1 Power Spectrum

The power spectrum is defined as follows. First, we find the auto-correlation function of the annihilation operator and then take the Fourier transform to go to the frequency domain[12]. Here S denotes the power spectrum.

$$S(\omega) = \int_{-\infty}^{\infty} dt e^{i\omega t} \langle a^\dagger(t) a(0) \rangle \tag{48}$$

Let the system with Hamiltonian $H = w_0 a^\dagger a$(SHO) be in a coherent state $|\alpha\rangle$. Let's calculate the power spectrum for the state.

$$\langle a^\dagger(t) a(0) \rangle = \langle e^{iHt} a^\dagger e^{-iHt} a \rangle \tag{49}$$

To get this, we have used the Heisenberg time evolution of the creation operator, Let's calculate the expectation value in a coherent state.

$$\langle a^\dagger(t) a(0) \rangle = \langle \alpha | e^{iHt} a^\dagger e^{-iHt} a | \alpha \rangle \tag{50}$$

Now using $a|\alpha\rangle = \alpha|\alpha\rangle$ and $e^{-iHt}|\alpha\rangle = |\alpha(t)\rangle = e^{\frac{-i\omega t}{2}} |\alpha e^{-i\omega t}\rangle$ we get,

$$\langle a^\dagger(t) a(0) \rangle = \langle \alpha | e^{iHt} a^\dagger e^{-iHt} \alpha | \alpha \rangle = \alpha \langle \alpha | e^{iHt} a^\dagger e^{\frac{-i\omega_0 t}{2}} | \alpha e^{-i\omega_0 t} \rangle \tag{51}$$

Now, using complex conjugates of the above two properties, we get,

$$\langle a^\dagger(t) a(0) \rangle = \alpha \langle \alpha e^{-i\omega_0 t} | e^{\frac{i\omega_0 t}{2}} a^\dagger e^{\frac{-i\omega_0 t}{2}} | \alpha e^{-i\omega_0 t} \rangle = \alpha \langle \alpha e^{-i\omega_0 t} | e^{\frac{i\omega_0 t}{2}} a^\dagger e^{\frac{-i\omega_0 t}{2}} | \alpha e^{-i\omega_0 t} \rangle \tag{52}$$

$$\langle a^\dagger(t)a(0)\rangle = \alpha\langle \alpha e^{-i\omega_0 t}|a^\dagger|\alpha e^{-i\omega_0 t}\rangle = |\alpha|^2 e^{-i\omega_0 t} \tag{53}$$

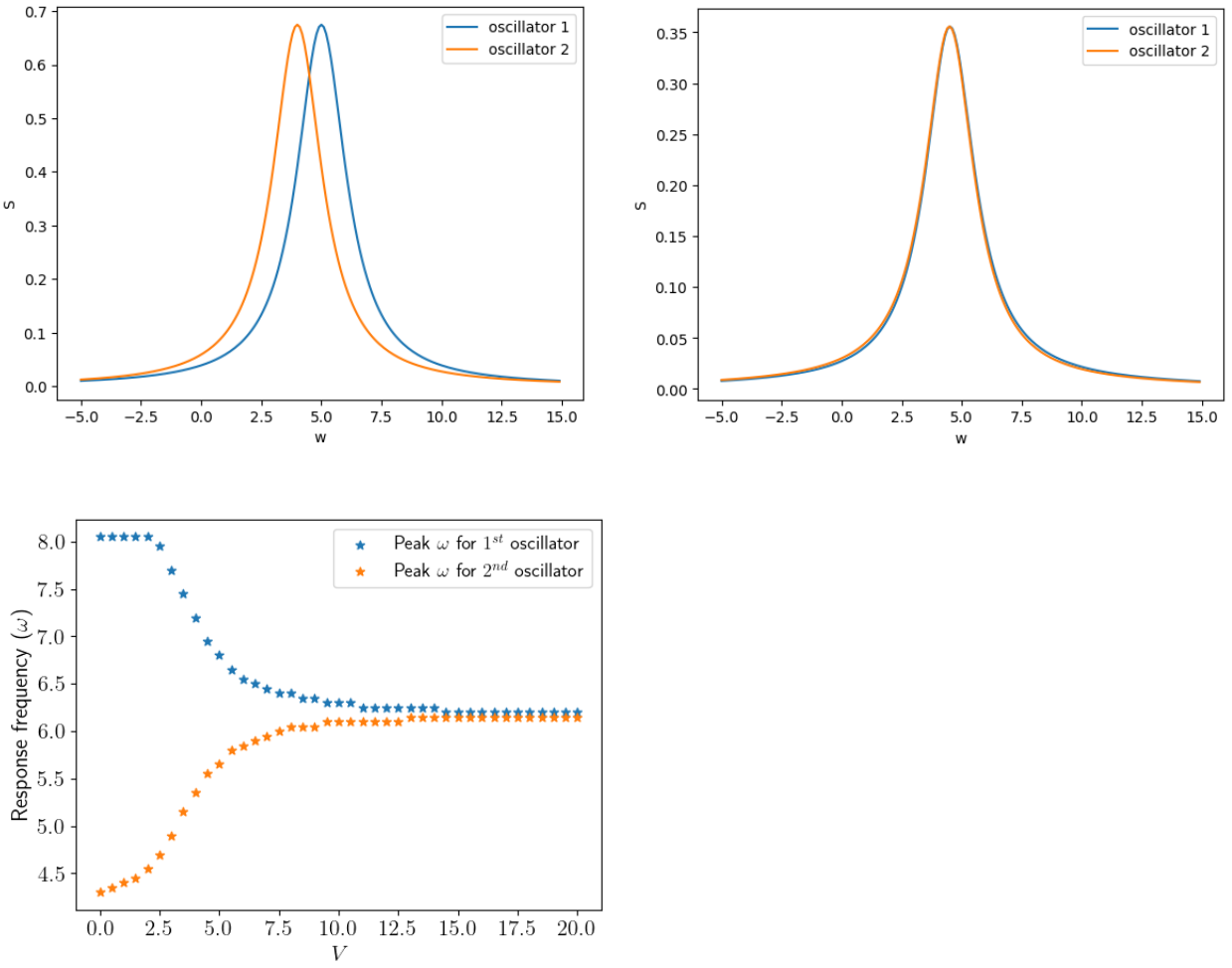

Figure 9: The figure shows relation between frequency distribution(as given by power spectrum) and coupling strength V in the quantum limit $\gamma_1 = 1.0 \ll \gamma_3 = 10.0$. The upper left is without coupling, the upper right is with coupling, and the Lower one shows the relation between peaks of the power spectrum and coupling strength.

Therefore, when we take the Fourier transform, we get the delta function with the peak at ω_0. This shows that the spectrum of the coherent state consists of only one frequency. But, when the state is not coherent, we will get a distribution over different frequencies. For a vdPo, the power spectrum is uni-modular, with the peak at the frequency ω_0 of the underlying SHO. (Hamiltonian of SHO as $H = \omega_0 a^\dagger a$).

Fig 9 shows the results when we couple two vdPos with different intrinsic frequencies and then

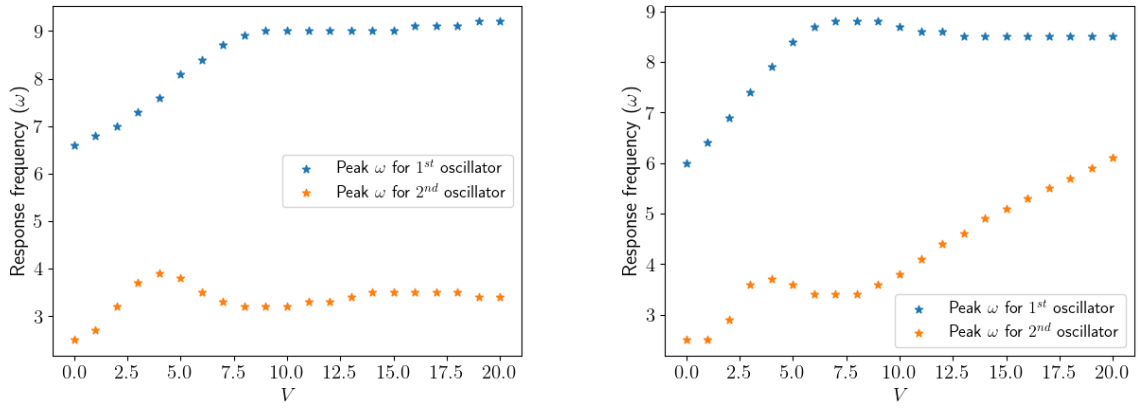

Figure 10: power spectrum showing frequency synchronization in the semi-classical limit in coupled vdPo

increase the coupling strength. The upper left shows the power spectrums of the two oscillators with district peaks, and the upper right shows that the distributions overlap, indicating that the oscillators have synchronised. The bottom figure shows the change in peaks of the distributions over coupling strength. As your peaks get closer and closer, we increase the coupling strength.

The power spectrum works well in the quantum limit because we have very few energy levels to deal with, but in classical limit calculations becomes computationally very expensive. So, in the semiclassical limit, we use a different order parameter, as shown in the next section. Fig. 10 shows peaks of the power spectrum with increasing coupling. While simulating, we need to cut off the number of SHO levels we will use. In high energy, demand on these levels increases. In the figure, the left one has 10 levels, and the right one has 13 levels. It is clear that we need to take a much higher number of levels, but that takes forever to simulate. The power spectrum works well in the quantum limit because we have very few energy levels to deal with, but in the semi-classical limit, calculations become computationally very expensive. So, in the semiclassical limit, we use different order parameter, as shown in the next section.

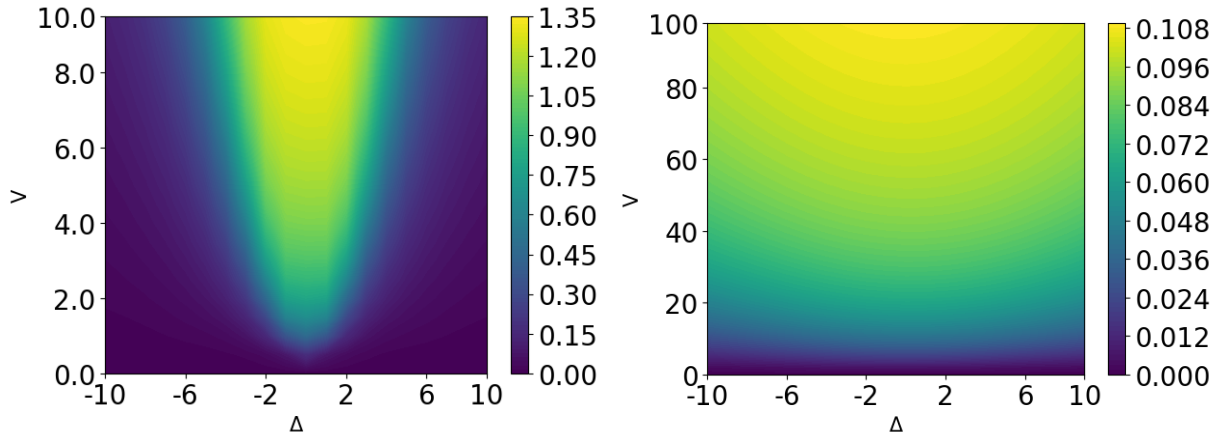

Figure 11: The figure shows the density plot for the synchronization order parameter as measured by the quantity $\min_{\delta^A,\delta^B} S(\rho||\delta^A \otimes \delta^B)$, Eq. (55) in the $V-\Delta$ plane in the semi-classical limit $\gamma_1 = 1.0 \gg \gamma_3 = 0.1$ (left panel) and in the quantum limit $\gamma_1 = 1.0 \ll \gamma_3 = 10.0$ (right panel).

3.2.2 Generalised measure of Synchornisation

As the name implies, this measure can be used on any system as shown in paper [5]. Let the density matrix in the steady state be given byρ, then the order parameter is given by,

$$\Omega(\rho) = \min_{\sigma\in\Sigma} S(\rho||\sigma) \tag{54}$$

where $S(\rho||\sigma) = Tr[\rho ln\rho - \rho ln\sigma]$ and Σ is a set of limit cycle states(i.e. the states which give rise whose Wigner function shows limit cycle). The choice of Σ depends on the system at hand. For our system, it is clear from the right side figure of Fig. 6 and Fig. 7 that diagonal matrices give a limit cycle. So, we will take the space of diagonal matrices as limit-cycle states. With this Σ the generalised measure can be written in a much more computable form. as follows,

$$\Omega(\rho) = \min_{\delta^A,\delta^B} S(\rho||\delta^A \otimes \delta^B) = S_{coh}(\rho) + I_c(\rho) \tag{55}$$

$$S_{coh}(\rho) = S(\rho_{diag}) - S(\rho), \qquad I_c(\rho) = S(\rho^A_{diag}) + S(\rho^B_{diag}) - S(\rho_{diag}) \tag{56}$$

The superscripts of A and B represent the partial density matrix of the first and second oscillators, respectively. As calculating this measure involves matrix manipulations, it is computationally feasible.

Fig. 11 show the results of the Generalised measure for the steady-state density matrix resulting from solving Eq. (44). In the semi-classical limit(left side of Fig. 11) looks similar to the Arnold tongue from classical vdPo(see Fig. 4). The difference is that the quantum case doesn't have a sharp boundary between synchronised and unsynchronized states. Instead, we get continuous changes in parameters going from lower to higher. This is because the system is quantum is nature, which inherently adds fluctuations. In the quantum limit, however (right side of Fig. 11), things are different. It is very difficult to synchronise quantum systems, requiring very high values of coupling strength.

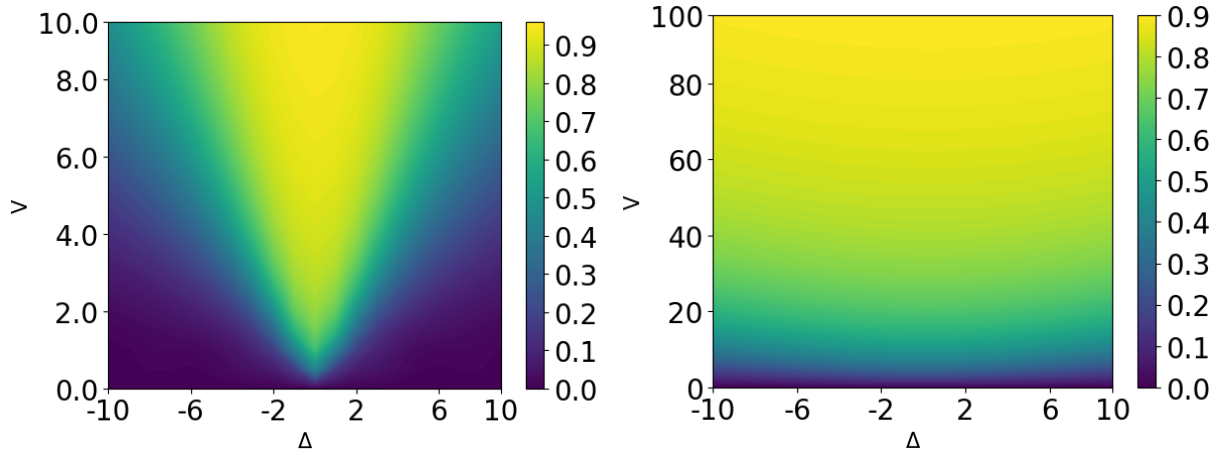

Figure 12: The figure shows the density plot for the synchronization order parameter as measured by the quantity R_{ph} in the $V-\Delta$ plane in the semi-classical limit $\gamma_1 = 1.0 \gg \gamma_3 = 0.1$ (left panel) and in the quantum limit $\gamma_1 = 1.0 \ll \gamma_3 = 10.0$ (right panel).

Measure of phase locking

Another measure for studying is called the measure of Phase locking, which following Ref. [13], we define for our system as $\langle \hat{a}_2^\dagger \hat{a}_1 \rangle$. The quantity $\langle \hat{a}_2^\dagger \hat{a}_1 \rangle$ gives a way to extract information about the phase difference between oscillators in the following way: For a coherent state, $\langle a_j \rangle \sim e^{i\phi_j}$, where $j = 1, 2$; so, $\langle \hat{a}_2^\dagger \hat{a}_1 \rangle \sim e^{i(\phi_2 - \phi_1)}$. The order parameter $R_{ph} = Re\left(\langle \hat{a}_2^\dagger \hat{a}_1 \rangle\right) = 1$ when system is completely phase-locked as $\phi_2 = \phi_1$. The lower the value of this order parameter, the lesser the degree of phase lock. We plot our results in Fig. 12. We observe the usual Arnold-tongue-like region of phase locking when $\gamma_1 \gg \gamma_3$, i.e. in the semi-classical regime. In the quantum regime, i.e. when $\gamma_3 \gg \gamma_1$, the Arnold tongue is replaced by a broad band-like region of phase locking.

Also, this band is obtained at a much greater value of the coupling strength V than the high energy limit.

Conclusion: Analysing the results from the power spectrum, Generalised measure and phase synchronisation, we conclude that in the Semi-classical(High energy) limit, the Arnold tongue is preserved. But in the quantum limit(low energy), this is replaced by a flat band. So, in the quantum limit, there is a threshold of coupling strength below which we don't see synchronisation. But once past the threshold, the system remains synchronised for larger values for detuning parameters. It is important to note that when studying quantum synchronisation, we can't depend on only one order parameter. Different order parameters that are efficient in different regions need to be used.

3.3 Non-markovian Correction to Lindblad Equation

Now, we turn to the second main result of the thesis. So far, all Open Quantum Systems used in the thesis had Lindbladian with Markovian approximation. In the derivation of Lindbladian, Markov Approximation comes in Eq. (22). We assume the bath correlation functions are delta functions. Realistically, bath correlation functions will have some finite width. In this section, we add a first-order correction to Lindbladian due to the width in correlation functions.

We will start with the same system as in Section 2.4, with the following Hamiltonian.

$$H_{Total} = H_S + H_B + H_I$$

$$H_S = \omega_0 a^\dagger a, \qquad H_B = \Sigma_k \omega_k b_k^\dagger b_k, \qquad H_I = a\Gamma^\dagger + a^\dagger \Gamma \qquad \Gamma = \Sigma_j \omega_j k_j b_j$$

Follow similar derivation till Eq. (20), and relations in Eq. (21) are still true.

$$\begin{aligned}\dot{\tilde{\rho}} = -\int_0^t dt' \{ &\left[\tilde{a}(t)\tilde{a}^\dagger(t')\tilde{\rho}(t') - \tilde{a}^\dagger(t')\tilde{\rho}(t')\tilde{a}(t)\right] \langle \tilde{\Gamma}^\dagger(t)\tilde{\Gamma}(t')\rangle_{bath} + H.C. \\ &+ \left[\tilde{a}^\dagger(t)\tilde{a}(t')\tilde{\rho}(t') - \tilde{a}(t')\tilde{\rho}(t')\tilde{a}^\dagger(t)\right] \langle \tilde{\Gamma}(t)\tilde{\Gamma}^\dagger(t')\rangle_{bath} + H.C.\}\end{aligned} \tag{57}$$

Here, I will assume the exponential form for bath correlations, but the same procedure can be followed for more complex ones. For more details, please refer to Appendix. **??**Let λ_1 and $_2$ be correlation lengths, and then we get the following correlation functions.

$$\begin{aligned}\langle \tilde{\Gamma}(t)\tilde{\Gamma}^\dagger(t')\rangle_{bath} &= \frac{R_1}{\lambda_1} e^{\frac{-(t-t')}{\lambda_1}} \\ \langle \tilde{\Gamma}^\dagger(t)\tilde{\Gamma}(t')\rangle_{bath} &= \frac{R_2}{\lambda_1} e^{\frac{-(t-t')}{\lambda_2}}\end{aligned} \tag{58}$$

For simplicity, let's evaluate only the first row in Eq. (57), the answer for the second row will be analogous to the first one.

$$\dot{\tilde{\rho}} = -\int_0^t dt' \left[\tilde{a}(t)\tilde{a}^\dagger(t')\tilde{\rho}(t') - \tilde{a}^\dagger(t')\tilde{\rho}(t')\tilde{a}(t)\right] \langle \tilde{\Gamma}^\dagger(t)\tilde{\Gamma}(t')\rangle_{bath} + H.C. \tag{59}$$

Let's do a change of variable as $t' = t - \tau$,we get

$$\dot{\tilde{\rho}} = -R_1 \int_0^t d\tau \left[\tilde{a}(t)\tilde{a}^\dagger(t-\tau)\tilde{\rho}(t-\tau) - \tilde{a}^\dagger(t-\tau)\tilde{\rho}(t-\tau)\tilde{a}(t)\right] \langle \tilde{\Gamma}^\dagger(t)\tilde{\Gamma}(t-\tau)\rangle_{bath} + H.C. \quad (60)$$

Now lets put $\tau' = \tau/\lambda_1$,

$$\dot{\tilde{\rho}} = -R_1 \int_0^{t/\lambda_1} \lambda_1 d\tau \left[\tilde{a}(t)\tilde{a}^\dagger(t-\lambda_1\tau')\tilde{\rho}(t-\lambda_1\tau') - \tilde{a}^\dagger(t-\lambda_1\tau')\tilde{\rho}(t-\lambda_1\tau')\tilde{a}(t)\right] \frac{1}{\lambda_1} e^{-\tau'} + H.C. \quad (61)$$

Now, Tayler expanding all the operators and ignoring terms with $O(\lambda_1^2)$. Now, evaluating this integral and going back to the Schrodinger Picture and evaluating the analogous integral of the second row in Eq. (57) we get the following equation. Please refer to the Appendix. **??** for derivation.

$$\begin{aligned}\dot{\rho} = &-i[H_s,\rho] + R_1 D[a^\dagger]\rho - \lambda_1 R_1 D[a^\dagger](D[a^\dagger]\rho) + R_2 D[a]\rho - \lambda_2 R_2 D[a]\,(D[a]\rho) \\ &+ i\lambda_1 R_1 \left(a[H_s,a^\dagger]\rho - [H_s,a^\dagger]\rho a + \rho[H_s,a]a^\dagger - a^\dagger\rho[H_s,a]\right) \\ &+ i\lambda_2 R_2 \left(a^\dagger[H_s,a]\rho - [H_s,a]\rho a^\dagger + \rho[H_s,a^\dagger]a - a\rho[H_s,a^\dagger]\right) \end{aligned} \quad (62)$$

Let's take a two-level system(we will use spin half in a Magnetic field, could be anything else) coupled to an external drive with Rotating wave approximation and also coupled to a bath. Let the corresponding Hamiltonian be as follows.

$$H = H_s + H_B + H_I \quad (63)$$

$$H_s = \hbar\omega_0\sigma_z + \Omega(e^{-i\omega_l t}\sigma_+ + e^{i\omega_l t}\sigma_-) \quad (64)$$

$$H_B = \Sigma_k \omega_k b_k^\dagger b_k, \qquad H_I = a\Gamma^\dagger + a^\dagger\Gamma \qquad \Gamma = \Sigma_j \omega_j k_j b_j \quad (65)$$

This system(Eq. (64)) can be solved with Lindblad Dynamics as in Eq .(24) and first-order correction as in Eq. (100). Fig. 13 shows Markovian dynamics with and drive. We have plotted the Husimi-Q function in the spin coherent basis. As you can see, when there is no drive, the Q function is uniform over ϕ (indicating limit cycle) and with a drive, it becomes non-uniform. Similarly, Fig. 14 shows the corresponding non-markovian dynamics. Q function without drive is again uniform, but the one with drive becomes less non-uniform. This type of behaviour strongly

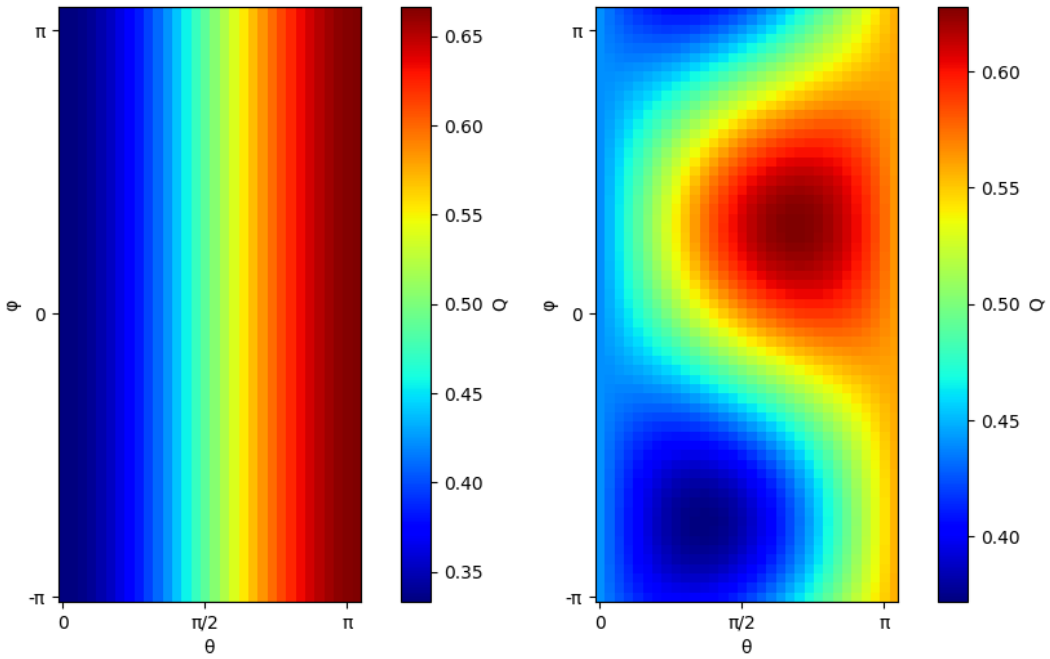

Figure 13: The figure shows Husimi-Q function for steady using Lindbladian(Markov) dynamics as in Eq. (24) for system in Eq. (64).Parameters for simulation are $R_1 = 1$, $R_2 = 2$, $\omega_0 = 0$, $\Omega = 0$ on left(Not coupled to drive) and $R_1 = 1$, $R_2 = 2$, $\omega_0 = 3$, $\Omega = 4$ on right (coupled to drive). Note that Husimi-Q is calculated in a Spin-coherent basis

indicates that non-markovian dynamics are detrimental to Synchronisation. However, because we haven't conducted a complete parameter swipe, we can't conclude with only this data. This can be a direction to work on in future.

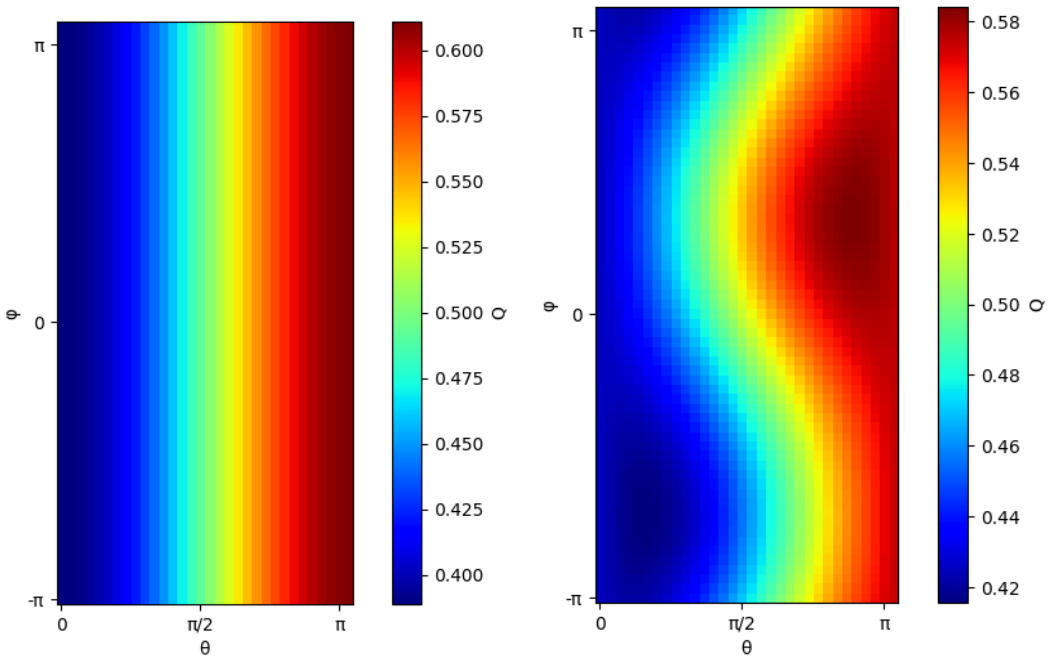

Figure 14: The figure shows Husimi-Q function for steady using Non-markovian dynamics as in Eq. (100) for system in Eq. (64).Parameters for simulation are $R_1 = 1$, $R_2 = 2$, $\omega_0 = 0$, $\Omega = 0$,$\lambda_1 = 0.2$, $\lambda_2 = 0.05$ on left(Not coupled to drive) and $R_1 = 1$, $R_2 = 2$, $\omega_0 = 3$, $\Omega = 4$,$\lambda_1 = 0.2$, $\lambda_2 = 0.05$ on right (coupled to drive). Note that Husimi-Q is calculated in a Spin-coherent basis

3.4 Conclusion and Future Directions

The synchronization of classical oscillators showing limit cycle behaviour has been a topic of interest for years, but the synchronisation of quantum oscillators having limit cycles has been getting more attention recently. We studied one such limit cycle oscillator. We showed that the quantum oscillator(namely Vanderpol) shows synchronisation (similar to classical vdPo) in a high energy limit called the semi-classical limit. However, the coupling strength required for synchronisation is more in the quantum(low energy) limit than in the classical case. So, it's difficult to synchronise the quantum oscillator with low energy. However, if enough coupling strength is given, the system remains Synchronised for larger values of the detuning parameter. It is worth noting that in the semi-classical limit, the Arnold Tongue is seen for the order parameter. But in the quantum limit, this is replaced by a band. The quantum oscillator, like its classical counterpart, also shows amplitude death with strong enough coupling.

In the second part, we showed a new way to solve the non-Markovian dynamics. We made a first-order correction to the Lindblad Master equation in terms of bath correlation time. Current data from non-Markovian dynamics shows that non-Markovian dynamics disrupt the Synchronisation. Future work could be along these lines to see the in-depth effect of non-Markovinan correction. Also, the equation that we got could be applied to any system, so it will be interesting to see the effect on spin-1. Applying this to VanderPol will be computationally difficult using the current simulation method. So, future work could be done along these to figure out how to solve the VanderPol oscillator with non-Markovian conditions.

Appendices

A Results on single and two coupled classical van der Pol oscillators

The equation of motion of a vdPo is given by

$$\ddot{x} + x - \varepsilon\dot{x} + \gamma_3 x^2\dot{x} = 0. \tag{66}$$

Here, ε and γ_3 correspond to coefficients of negative and nonlinear damping, respectively. We can make two first-order differential equations from the above second-order equation as,

$$\begin{aligned} \dot{x} &= y, \\ \dot{y} &= -x + \varepsilon\dot{x} - \gamma_3 x^2\dot{x}. \end{aligned} \tag{67}$$

To get an equation of the complex amplitude α, we write $\alpha(t) = x(t) + \mathrm{i}y(t)$. We then find $\dot{\alpha}$ by using Eq.‘(67) and carry out Krylov–Bogoliubov averaging as outlined in [10] to get the following amplitude equation

$$\dot{\alpha} = -\mathrm{i}\omega\alpha + \alpha(\frac{\varepsilon}{2} - \frac{\gamma_3}{8}|\alpha|^2); \;\; \varepsilon > 0, \gamma_3 > 0. \tag{68}$$

Again, following Ref. [10] the amplitude equation for two diffusively coupled vdPO will be given by

$$\dot{\alpha}_1 = -\mathrm{i}\omega_1\alpha_1 + \alpha_1(\frac{\varepsilon}{2} - \frac{\gamma_3}{2}|\alpha_1|^2) + (\alpha_2 - \alpha_1)V, \tag{69}$$

$$\dot{\alpha}_2 = -\mathrm{i}\omega_2\alpha_2 + \alpha_2(\frac{\varepsilon}{2} - \frac{\gamma_3}{2}|\alpha_2|^2) + (\alpha_1 - \alpha_2)V. \tag{70}$$

Here, ω_1 and ω_2 are the frequencies of the two vdPos while V is the strength of diffusive coupling. We now convert to polar coordinates by making the following substitution

$$\alpha_n = r_n e^{\mathrm{i}\theta_n};\ \ n = 1,2, \tag{71}$$

in Eqs. (69)–(70) to get

$$\dot{r}_1 = r_1\left(\frac{\varepsilon}{2} - \frac{\gamma_3}{2}r_1^2\right) - (r_1 - r_2\cos\theta)V, \tag{72}$$

$$\dot{r}_2 = r_2\left(\frac{\varepsilon}{2} - \frac{\gamma_3}{2}r_2^2\right) - (r_2 - r_1\cos\theta)V, \tag{73}$$

$$\dot{\theta} = -\Delta - \left(\frac{r_1}{r_2} + \frac{r_2}{r_1}\right)V\sin\theta;\ \theta \equiv \theta_2 - \theta_1, \Delta = \omega_2 - \omega_1. \tag{74}$$

Here Δ is called the detuning parameter. Performing the linear stability analysis of the fixed points of Eqs. (72)– (74) gives us an Arnold tongue-like region in the $V - \Delta$ plane where the system is synchronized [10].

B Semi-classical analysis using the Fokker-Planck equation

In this appendix, starting from the Lindblad equation Eq. (44), we will get the time evolution for the Wigner distribution in the form of the Fokker-plank equation. The method we follow is outlined in greater detail in chapter 3 and chapter 4 of Ref. [3]. We define a characteristic function

$$\chi_s(\mathbf{z}) \equiv \mathrm{Tr}\left[\rho \exp\left(iz_1^*\hat{a}_1^\dagger + iz_1\hat{a}_1\right)\exp\left(iz_2^*\hat{a}_2^\dagger + iz_2\hat{a}_2\right)\right], \tag{75}$$

where we have $\mathbf{z} = (z_1, z_1^*, z_2, z_2^*)$. We then note that the Wigner function $W(\alpha)$ of the system, with $\alpha \equiv (\alpha_1, \alpha_1^*, \alpha_2, \alpha_2^*)$, in terms of the characteristic function χ_s is given by the following Fourier transform:

$$W(\alpha) = \left(\frac{1}{\pi}\right)^4 \int d^2z_1 d^2z_2 \chi_s(\mathbf{z}) \exp\left(-\mathrm{i}z_1^*\alpha_1^* - \mathrm{i}z_1\alpha_1 - \mathrm{i}z_2^*\alpha_2^* - \mathrm{i}z_2\alpha_2\right). \tag{76}$$

Now taking time derivative of Eq. (75) we get

$$\dot{\chi}_s(\mathbf{z}) = \mathrm{Tr}\left[\dot{\rho} \exp\left(iz_1^*\hat{a}_1^\dagger + iz_1\hat{a}_1\right)\exp\left(iz_2^*\hat{a}_2^\dagger + iz_2\hat{a}_2\right)\right]. \tag{77}$$

We then substitute for $\dot{\rho}$ from Eq. (44) and arrive at the following equation:

$$\begin{aligned}
\dot{\chi}_s(\mathbf{z}) = \sum_{j=1}^{2} \Bigg[& \left(i\omega_j(iz_j)\frac{\partial}{\partial(iz_j)} - i\omega_j(iz_j^*)\frac{\partial}{\partial(iz_j^*)}\right) + \frac{\gamma_1}{2}\left(-|z|^2 + (iz_j)\frac{\partial}{\partial(iz_j)} + (iz_j) + (iz_j^*)\frac{\partial}{\partial(iz_j^*)}\right) \\
& - \frac{V}{2}\left(|z|^2 + (iz_j)\frac{\partial}{\partial(iz_j)} + (iz_j) + (iz_j^*)\frac{\partial}{\partial(iz_j^*)}\right) + \frac{V}{2}\left(-(iz_j)(iz_{j'}^*) + (iz_j)\frac{\partial}{\partial(iz_{j'})} + (iz_j^*)\frac{\partial}{\partial(iz_{j'}^*)}\right) \\
& + \gamma_3\Bigg(4(iz_j)^2\frac{\partial}{\partial(iz_j)^2} + 8(iz_j)^2\frac{\partial}{\partial iz_j^*}\frac{\partial}{\partial iz_j} - 8(iz_j)(iz_j^*)\frac{\partial^2}{\partial^2 iz_j^*} - 8(iz_j)(iz_j^*)\frac{\partial^2}{\partial^2 iz_j} - 24(iz_j)(iz_j^*)\frac{\partial}{\partial iz_j^*}\frac{\partial}{\partial iz_j} \\
& + 4(iz)\frac{\partial}{\partial^3(iz_j)} + 4(iz_j)\frac{\partial}{\partial^2 iz_j}\frac{\partial}{\partial iz_j} + 8(iz)\frac{\partial}{\partial iz_j^*}\frac{\partial}{\partial^2 iz} + 4z_j^{*2}\frac{\partial^2}{\partial^2 iz_j^*} + 8z_j^{*2}\frac{\partial}{\partial iz_j^*}\frac{\partial}{\partial iz_j} + 4iz_j^*\frac{\partial^3}{\partial^3 iz_j^*} \\
& + 8z_j^*\frac{\partial^2}{\partial^2 iz_j^*}\frac{\partial}{\partial iz_j} + 4iz^*\frac{\partial}{\partial iz_j^*}\frac{\partial^2}{\partial^2 iz_j} + \mathscr{O}(z_j)\Bigg)\Bigg]\chi_s(\mathbf{z}).
\end{aligned} \tag{78}$$

Here, j' implies $j' = 2$ when $j = 1$ and $j' = 1$ when $j = 2$. From Eq. (76), we see that α_j is the Fourier-conjugated variable for z_j. Terms that scale as z_j in Eq. (78) will scale as $1/\alpha_j$ as we go

from the characteristic function (χ_s) to the Wigner function $W(\alpha)$. In the semiclassical limit, α_j is large and hence $1/\alpha_j$ will be small. Thus, we may ignore $\mathscr{O}\left(z_j\right)$ terms in Eq. (78). We then substitute $\dot{\chi}_s(\mathbf{z})$ in the time derivative of Eq. (76), and after a bit of algebra, as outlined in Ref. [3], we have the following Fokker–Planck equation for $W(\alpha)$:

$$\begin{aligned}\frac{\partial W(\alpha)}{\partial t} = \sum_{j=1}^{2}\Bigg[-\left(\partial_{\alpha_j}\mu_{\alpha_j}+c.c.\right)+\frac{1}{2}\Bigg(\frac{\partial^2 D_{\alpha_j^2}}{\partial\alpha_j^2} \\ + \frac{\partial^2 D_{\alpha*_j^2}}{\partial\alpha*_j^2}+\frac{\partial^2 D_{\alpha_j\alpha*_j}}{\partial\alpha_j\partial\alpha*_j}+\frac{\partial^2 D_{\alpha_j\alpha*'_j}}{\partial\alpha_j\partial\alpha*'_j}\Bigg)\Bigg]W(\alpha),\end{aligned} \tag{79}$$

where the drift coefficients and the diffusion coefficients are respectively given by

$$\begin{aligned}\mu_{\alpha_j} &= \left(-i\omega_j+\frac{\gamma_1}{2}-\frac{V}{2}\right)\alpha_j+\frac{V}{2}\alpha_{j'}, \\ &\quad -\frac{\gamma_3}{2}\left(\alpha^3+\alpha^*|\alpha|^2+2\alpha|\alpha|^2\right), \\ D_{\alpha_j\alpha_j^*} &= \gamma_1+V+\frac{\gamma_3}{2}\left(\alpha_j^{*2}+\alpha^2+3|\alpha|^2\right), \\ D_{\alpha_j\alpha*_{j'}} &= V, \\ D_{\alpha_j}^2 &= \frac{-\gamma_3}{2}\left(\alpha^2+2|\alpha|^2\right), \\ D_{\alpha_j^{*2}} &= c.c.\text{ of } D_{\alpha_j^2}.\end{aligned} \tag{80}$$

We now change variables to cartesian coordinates $\mathbf{X}\equiv(x_1,x_2,y_1,y_2)$ by substituting α_j as x_j+iy_j to rewrite Eq. (79) as

$$\begin{aligned}\frac{\partial W(\mathbf{X})}{\partial t} = \sum_{j=1}^{2}\Bigg[-\left(\frac{\partial\mu_{x_j}}{\partial x_j}+\frac{\partial\mu_{y_j}}{\partial y_j}\right) \\ + \frac{1}{2}\Bigg(\frac{\partial^2 D_{x_jx_j}}{\partial x_j\partial x_j}+\frac{\partial^2 D_{y_jy_j}}{\partial y_j\partial y_j}+\frac{\partial^2 D_{x_jx'_j}}{\partial x_j\partial x'_j} \\ + \frac{\partial^2 D_{y_jy'_j}}{\partial y_j\partial y'_j}+\frac{\partial^2 D_{x_jy_j}}{\partial x_j\partial y_j}\Bigg)\Bigg]W(\mathbf{X}),\end{aligned} \tag{81}$$

In Eq. (81), $\mu \equiv (\mu_{x_1}, \mu_{x_2}, \mu_{y_1}, \mu_{y_2})$ is the drift vector and $\mathbf{D}$ is the diffusion matrix, which can be explicitly written as

$$\begin{aligned} \mu_{x_j} &= \omega_j y_j + \left(\frac{\gamma_1}{2} - 2\gamma_3 x_j^2 - \frac{V}{2}\right) x_j + \frac{V}{2} x_j', \\ \mu_{y_j} &= -\omega_j x_j + \left(\frac{\gamma_1}{2} - 2\gamma_3 x_j^2 - \frac{V}{2}\right) y_j + \frac{V}{2} y_j', \end{aligned} \tag{82}$$

and

$$\begin{aligned} \mathbf{D} &\equiv \begin{bmatrix} D_{x_1x_1} & D_{x_1y_1} & D_{x_1x_2} & 0 \\ D_{y_1x_1} & D_{y_1y_1} & 0 & D_{y_1y_2} \\ D_{x_2x_1} & 0 & D_{x_2x_2} & D_{x_2y_2} \\ 0 & D_{y_2y_1} & D_{y_2x_2} & D_{y_2y_2} \end{bmatrix} \\ &= \frac{1}{2} \begin{bmatrix} \kappa_1 & 4x_1y_1 & -\frac{V}{2} & 0 \\ 4x_1y_1 & \kappa_2 & 0 & -\frac{V}{2} \\ -\frac{V}{2} & 0 & \kappa_3 & 4x_1y_1 \\ 0 & -\frac{V}{2} & 4x_1y_1 & \kappa_4 \end{bmatrix}. \end{aligned} \tag{83}$$

Here, $\kappa_1 \equiv \gamma_1/2 + V/2 + \gamma_3\left(2x_1^2\right)$, $\kappa_2 \equiv \gamma_1/2 + V/2 + \gamma_3\left(8x_1^2 + 2y_1^2\right)$, $\kappa_3 \equiv \gamma_1/2 + V/2 + \gamma_3\left(2x_2^2\right)$, and $\kappa_4 \equiv \gamma_1/2 + V/2 + \gamma_3\left(8x_2^2 + 2y_2^2\right)$. The next step involves solving numerically the stochastic differential equation corresponding to Eq. (81) given by

$$d\mathbf{X} = \mu dt + \sigma d\mathbf{W}_t, \tag{84}$$

where $\mathbf{W}_t$ is the Wiener process. Here μ is explicitly given by Eq. (82) while the matrix σ is obtained from $\mathbf{D}$ in the following way: We first compute the eigenvalues $(\lambda_1, \lambda_2, \lambda_3, \lambda_4)$ and eigenvectors $(\mathbf{v}_1, \mathbf{v}_2, \mathbf{v}_3, \mathbf{v}_4)$ of $\mathbf{D}$. One has to note that each eigenvector of $\mathbf{D}$ is a column vector with four elements. Then, we construct a 4×4 unitary matrix $\mathbf{U} = [\mathbf{v}_1, \mathbf{v}_2, \mathbf{v}_3, \mathbf{v}_4]$ and another 4×4 diagonal matrix $\mathbf{D}'$ whose diagonal elements are the eigenvalues of $\mathbf{D}$. The matrix σ is then given by $\sigma = \mathbf{U}\sqrt{\mathbf{D}'}\mathbf{U}^{-1}$. In this paper, we compute σ numerically at each time step by numerically

computing the eigenvalues and eigenvectors of $\mathbf{D}$. Thus, σ is updated in each time step and then used in Eq. (84), which in turn is numerically integrated using the Euler–Maruyama algorithm [7] to obtain the value of $\mathbf{X}$ at the next time step; σ is computed again, and the process repeats.

C Mapping the system (37) to classical vdPo

In this appendix, we map Eq. (37) to the classical vdPo equation given by:

$$\ddot{x} + x - \varepsilon\dot{x} + \gamma_3 x^2\dot{x} = 0. \tag{85}$$

Note that this is the same as Eq. (26) when you put in parameters for vdPo. Here, ε and γ_3 are the parameters that control the negative and the nonlinear dissipation, respectively. As outlined in Ref. [1], writing $x = x_0 + \varepsilon x_1 + \ldots$, with $x_0 = Ae^{it}$; $A \in \mathbb{C}$, and with the approximation that the time variation in the amplitude A being slow as compared to the time scale of oscillation of the system, the amplitude equation for the vdPo above will be given by

$$\frac{dA}{dt} = \frac{1}{2}\left(1 - \frac{|A|^2}{4\mathscr{A}_c^2}\right)A, \tag{86}$$

where $\mathscr{A}_c = \sqrt{\frac{\varepsilon}{\gamma_3}}$. The steady-state amplitude of oscillations of the vdPo is then given by $|A| = 2\mathscr{A}_c$, obtained by putting the LHS of Eq. (86) to zero. To better compare the classical vdPo with the quantum model given by Eq. (37), let us write Eq. (85) in terms of $\mathscr{A}_c$, to get

$$\ddot{x} + x - \varepsilon\left(1 - \frac{x^2}{\mathscr{A}_c^2}\right)\dot{x} = 0. \tag{87}$$

We now outline the steps to obtain the vdPo in the classical(high energy) limit starting from the quantum vdPo in Eq. (37). First, let us identify α as the eigenvalue of the coherent state of the quantum harmonic oscillator, implying $\langle\hat{a}\rangle = \alpha$, where $\hat{a}$ is the usual annihilation operator for the quantum harmonic oscillator. The next step is to compute the quantity $d\langle\hat{a}\rangle/dt$. Using the standard relation $\langle\hat{a}\rangle = \mathrm{Tr}[\rho\hat{a}]$, we get

$$\frac{d\langle\hat{a}\rangle}{dt} = \mathrm{Tr}\left[\dot{\rho}\hat{a}\right]. \tag{88}$$

We now substitute for $\dot{\hat{\rho}}$ from Eq. (37) in Eq. (88), use $\langle\hat{a}\rangle = \alpha$, and invoke an approximation valid in the semi-classical regime. To this end, let us note that $\langle\hat{x}^2\hat{a}\rangle = (1/2)\langle\hat{a}^3 + (\hat{a}^\dagger)^2\hat{a} + 2\hat{a}^\dagger\hat{a}^2 + \hat{a}\rangle = (1/2)(\alpha^3 + (\alpha^*)^2\alpha + 2\alpha^*\alpha^2 + \alpha)$. In the semi-classical regime, one would have to consider large values of $|\alpha|$ [4], in which case one may in the last equality above keep only the nonlinear terms in α, to obtain $\langle\hat{x}^2\hat{a}\rangle \approx \alpha(1/2)(\alpha^2 + (\alpha^*)^2 + 2\alpha^*\alpha) = \langle\hat{x}\rangle^2\alpha$. We then arrive at the following

equation:

$$\langle \dot{x} \rangle = \frac{\varepsilon}{2}\left(1 - \frac{\langle x \rangle^2}{2A_c^2}\right)\langle x \rangle + \langle p \rangle, \tag{89}$$

$$\langle \dot{p} \rangle = \frac{\varepsilon}{2}\left(1 - \frac{\langle x \rangle^2}{2A_c^2}\right)\langle p \rangle - \langle x \rangle, \tag{90}$$

where, $\varepsilon = \gamma_1 - \gamma_2$. Now taking another time derivative of Eq. (89) and substituting $\langle \dot{p} \rangle$ from Eq. (90), we get the following equation:

$$\langle \ddot{x} \rangle + \langle x \rangle = \varepsilon\left(1 - \frac{\langle x \rangle^2}{A^2}\right)\langle \dot{x} \rangle + \mathscr{O}\left(\varepsilon^2\right). \tag{91}$$

On comparing the above equation with Eq. (87) we find that (91) is the classical van der Pol oscillator upto $\mathscr{O}\left(\varepsilon^2\right)$. So, if we compare between Eq. (28) and Eq. (37) , non-linearity parameter ε maps to $\gamma_1 - \gamma_2$ and A_c maps to $\sqrt{\frac{\gamma_1 - \gamma_2}{\gamma_3}}$.

D Derivation of non-Markovian Correction

Recall how we got Eq. (61) from Eq. (20), remember we are only solving the first row of Eq. (20), rewriting the same equation again,

$$\dot{\tilde{\rho}} = -\int_0^{t/\lambda_1} d\tau \left[\tilde{a}(t)\tilde{a}^\dagger(t - \lambda_1\tau')\tilde{\rho}(t - \lambda_1\tau') - \tilde{a}^\dagger(t - \lambda_1\tau')\tilde{\rho}(t - \lambda_1\tau')\tilde{a}(t)\right] e^{-\tau'} + H.C. \tag{92}$$

Now, Tayler is expanding all the operators as follows: from now on, if no time argument is given, then take it to t.

$$\tilde{a}^\dagger(t - \lambda_1\tau') = \tilde{a}^\dagger(t) - \lambda_1\tau'\frac{d\tilde{a}^\dagger(t)}{dt} \tag{93}$$

$$\tilde{a}(t - \lambda_1\tau') = \tilde{a}(t) - \lambda_1\tau'\frac{d\tilde{a}(t)}{dt} \tag{94}$$

$$\tilde{\rho}(t - \lambda_1\tau') = \tilde{\rho}(t) - \lambda_1\tau'\frac{d\tilde{\rho}(t)}{dt} \tag{95}$$

We are assuming $\lambda_1 \to 0$, so the integral goes to infinity, and we only keep the first term in the Tayler expansion. Substitute everything back and ignore $O(\lambda_1^2)$ to get:

$$\dot{\tilde{\rho}} = -\tilde{a}[\tilde{a} - \lambda_1(\tilde{a}^\dagger\dot{\tilde{\rho}} + \dot{\tilde{a}}^\dagger\tilde{\rho})] + [\tilde{a}^\dagger\tilde{\rho} - \lambda_1(\tilde{a}^\dagger\dot{\tilde{\rho}} + \dot{\tilde{a}}^\dagger\tilde{\rho})]\tilde{a} - [\tilde{\rho}\tilde{a} - \lambda_1(\dot{\tilde{\rho}} + \tilde{\rho}\dot{\tilde{a}})]\tilde{a}^\dagger + \tilde{a}^\dagger[\tilde{\rho}\tilde{a} - \lambda_1(\dot{\tilde{a}} + \tilde{\rho}\dot{\tilde{a}})] \tag{96}$$

Note: in the above equation whole RHS will be multiplied by the integral of the exponential(which comes out to be equal to 1). If we had chosen any other form of correlation, the integral would be a different number, not affecting the derivation. Keep this in mind: in the final step, I will multiply everything by R_1 representing the integral. Adding all the terms, we get:

$$\dot{\tilde{\rho}} = D[\tilde{a}^\dagger]\tilde{\rho} + \lambda_1\left(\tilde{a}\dot{\tilde{a}}^\dagger\tilde{\rho} - \dot{\tilde{a}}^\dagger\tilde{\rho}\tilde{a} + \tilde{\rho}\dot{\tilde{a}}\tilde{a}^\dagger - \tilde{a}^\dagger\tilde{\rho}\dot{\tilde{a}}\right) - \lambda_1 D[\tilde{a}^\dagger](\dot{\tilde{\rho}}) \tag{97}$$

$$\left(I + \lambda_1 D[\tilde{a}^\dagger]\right)\dot{\tilde{\rho}} = D[\tilde{a}^\dagger]\tilde{\rho} + \lambda_1\left(\tilde{a}\dot{\tilde{a}}^\dagger\tilde{\rho} - \dot{\tilde{a}}^\dagger\tilde{\rho}\tilde{a} + \tilde{\rho}\dot{\tilde{a}}\tilde{a}^\dagger - \tilde{a}^\dagger\tilde{\rho}\dot{\tilde{a}}\right) \tag{98}$$

Now multiply both sides by $\left(I - \lambda_1 D[\tilde{a}^\dagger]\right)$ and ignore $O(\lambda_1^2)$.

$$\dot{\tilde{\rho}} = D[\tilde{a}^\dagger]\tilde{\rho} + \lambda_1\left(\tilde{a}\dot{\tilde{a}}^\dagger\tilde{\rho} - \dot{\tilde{a}}^\dagger\tilde{\rho}\tilde{a} + \tilde{\rho}\dot{\tilde{a}}\tilde{a}^\dagger - \tilde{a}^\dagger\tilde{\rho}\dot{\tilde{a}}\right) + \lambda_1 D[\tilde{a}^\dagger]\left(D[\tilde{a}^\dagger]\tilde{\rho}\right) \tag{99}$$

Now, go back to Shrodinger picture using $U\dot{\tilde{O}}U^{-1} = i[H_S, O] + \dot{O}$, where $U = e^{iH_S t}$. Remember, $\dot{O} = 0$ for a and $a^\dagger$.

$$\begin{aligned}\dot{\rho} = &-i[H_s, \rho] + R_1 D[a^\dagger]\rho - \lambda_1 R_1 D[a^\dagger](D[a^\dagger]\rho) \\ &+ i\lambda_1 R_1\left(a[H_s, a^\dagger]\rho - [H_s, a^\dagger]\rho a + \rho[H_s, a]a^\dagger - a^\dagger\rho[H_s, a]\right)\end{aligned} \tag{100}$$

Now follow a similar procedure for the second Eq. (20) to the Eq. (100).

References

[1] Lior Ben Arosh, M. C. Cross, and Ron Lifshitz. Quantum limit cycles and the rayleigh and van der pol oscillators. *Phys. Rev. Res.*, 3:013130, Feb 2021.

[2] Heinz-Peter Breuer and Francesco Petruccione. *The Theory of Open Quantum Systems*. Oxford University Press, 01 2007.

[3] Howard J. Carmichael. *Statistical Methods in Quantum Optics 1*. Springer Berlin Heidelberg, 1999.

[4] Claude Cohen-Tannoudji, Bernard Diu, and Frank Laloe. Quantum mechanics, volume 1. *Quantum Mechanics*, 1, chapter 5, 1986.

[5] Noufal Jaseem, Michal Hajdušek, Parvinder Solanki, Leong-Chuan Kwek, Rosario Fazio, and Sai Vinjanampathy. Generalized measure of quantum synchronization. *Phys. Rev. Res.*, 2:043287, Nov 2020.

[6] J.R. Johansson, P.D. Nation, and Franco Nori. Qutip 2: A python framework for the dynamics of open quantum systems. *Computer Physics Communications*, 184(4):1234–1240, 2013.

[7] Peter E. Kloeden and Eckhard Platen. *Numerical Solution of Stochastic Differential Equations*. Springer Berlin Heidelberg, 1992.

[8] Tony E. Lee, Ching-Kit Chan, and Shenshen Wang. Entanglement tongue and quantum synchronization of disordered oscillators. *Phys. Rev. E*, 89:022913, Feb 2014.

[9] Tony E. Lee and H. R. Sadeghpour. Quantum synchronization of quantum van der pol oscillators with trapped ions. *Phys. Rev. Lett.*, 111:234101, Dec 2013.

[10] Arkady Pikovsky, Michael Rosenblum, and Jürgen Kurths. *Synchronization: A Universal Concept in Nonlinear Sciences*. Cambridge Nonlinear Science Series. Cambridge University Press, 2001.

[11] J M Radcliffe. Some properties of coherent spin states. *Journal of Physics A: General Physics*, 4(3):313, may 1971.

[12] Stefan Walter, Andreas Nunnenkamp, and Christoph Bruder. Quantum synchronization of a driven self-sustained oscillator. *Phys. Rev. Lett.*, 112:094102, Mar 2014.

[13] Talitha Weiss, Andreas Kronwald, and Florian Marquardt. Noise-induced transitions in optomechanical synchronization. *New Journal of Physics*, 18(1):013043, jan 2016.

[14] E. Wigner. On the quantum correction for thermodynamic equilibrium. *Phys. Rev.*, 40:749–759, Jun 1932.